Interfering With Hyaluronic Acid Metabolism Suppresses Glioma Cell Proliferation by Regulating Autophagy

Tao Yan
First Affiliated Hospital of Harbin Medical University
Xin Chen
First Affiliated Hospital of Harbin Medical University
Hua Zhan
First Affiliated Hospital of Harbin Medical University
Penglei Yao
First Affiliated Hospital of Harbin Medical University
Ning Wang
First Affiliated Hospital of Harbin Medical University
He Yang
First Affiliated Hospital of Harbin Medical University
Cheng Zhang
North Broward Preparatory School
Kaikai Wang
Zhejiang University School of Medicine Second Affiliated Hospital
Jingxian Sun
First Affiliated Hospital of Harbin Medical University
Yu Dong
Shenzhen Samii Medical Center
Enzhou Lu
First Affiliated Hospital of Harbin Medical University
Xingzhi Zheng
First Affiliated Hospital of Harbin Medical University
Ruotian Zhang
First Affiliated Hospital of Harbin Medical University
Xiaoxiong Wang
First Affiliated Hospital of Harbin Medical University
Jichao Ma
Biomolecular Science Center, Burnett College of Biomedical Sciences,University of Central Florida
Ming Gao

First Affiliated Hospital of Harbin Medical University

Junyi Ye

First Affiliated Hospital of Harbin Medical University

Xinzhuang Wang

First Affiliated Hospital of Harbin Medical University

Lei Teng

First Affiliated Hospital of Harbin Medical University

Huailei Liu

First Affiliated Hospital of Harbin Medical University

Shiguang Zhao (guangsz@hotmail.com)

First Affiliated Hospital of Harbin Medical University

Research

Keywords: Glioma, Hyaluronic acid, Autophagy, HAS3, CD44, 4-Methylumbelliferone

Posted Date: October 9th, 2020

DOI: https://doi.org/10.21203/rs.3.rs-88666/v1

Version of Record: A version of this preprint was published at Cell Death & Disease on May 1st, 2021. See the published version at https://doi.org/10.1038/s41419-021-03747-z.

Abstract

Background

The tumor microenvironment plays an important role in tumor progression. Hyaluronic acid (HA), an important component of the extracellular matrix in the tumor microenvironment, abnormally accumulates in a variety of tumors. Whereas the role of abnormal HA metabolism in glioma remains unclear.

Methods

The expression level of hyaluronic acid (HA) was analyzed by ELISA assay and proteins such as HAS3, CD44, P62, LC3, CCND1 and CCNB1 were measured with Western blot analysis. The cell viability and proliferation were measured by MTT and KI67 immunofluorescence staining respectively. Autophagic vesicles and autophagosomes were quantified by transmission electron microscopy (TEM) and GFP-RFP-LC3 fluorescence analysis respectively. Cell cycle was analyzed by flowcytometry and Western blot analysis. Immunohistochemical (IHC) staining was used to detect expression levels of HA, Ki67, HAS3 and CD44 in human and mouse tumor tissues. Lentivirus constructed HAS3 and CD44 knockout stable glioma cells were transplanted to BALB/C nude mice for in vivo experiments. 4-Methylumbelliferone (4MU) was also used to treat glioma bearing mice for verifing its anti-tumor ability. The expression curve of HAS3, CD44 and the disease-free survival (DFS) curves for HAS3, CD44 in patients with LGG and GBM was performed based on TCGA database.

Results

As shown in the present study, HA, hyaluronic acid synthase 3 (HAS3) and a receptor of HA named CD44 are expressed at high levels in human glioma tissues and negatively correlated with the prognosis of patients with glioma. Silencing HAS3 or blocking CD44 inhibited the proliferation of glioma cells in vitro and in vivo. The underlying mechanism was attributed to the inhibition of autophagy flux and further maintaining glioma cell cycle arrest in G1 phase. More importantly, 4-Methylumbelliferone (4-MU), a small competitive inhibitor of UDP with the ability to penetrate the blood-brain barrier (BBB), also inhibited the proliferation of glioma cells in vitro and in vivo.

Conclusion

Approaches that interfere with HA metabolism by altering the expression of HAS3 and CD44 and the administration of 4-MU potentially represent effective strategies for glioma treatment.

Background

Glioma is the most common intracranial malignant tumor. Although patients undergo adjuvant chemotherapy and radiotherapy after surgical resection, the survival time of patients is still short and the disability rate is high[1]. A better understanding of the mechanism and development of tumorigenesis is very important for effectively controlling the progression of glioma. The tumor microenvironment is a key

factor contributing to cancer cell survival, and it is a regulatory network composed of many cells and factors that maintain the growth of tumor cells[2]. In conclusion, strategies targeting the tumor microenvironment and its mediators effectively inhibit the growth of tumor cells[3].

Hyaluronic acid (HA) is an important extracellular matrix component in the tumor microenvironment[4]. HA is a linear polysaccharide consisting of D-glucuronic acid and N-acetyl-D-glucosamine[5]. HA is derived from the secretions of tumor cells or the interaction between tumor cells and stromal cells and is present at high levels in the microenvironment of many types of tumors[6]. HA family involved high molecular weight (HMW) HA (>1000000 Da), low molecular weight (LMW) HA and oligosaccharides (o-HA) (∼400–20000 Da). LMW-HA refers to HA with a molecular weight between HMW-HA and o-HA. HMW-HA can be degraded into LMW-HA or o-Ha when the body is subjected to an injury or a pathological insult, such as cancer[7]. HAs of different molecular weights exert different biological functions; for instance, HMW-HA possesses antiangiogenic and immunosuppressive activities, whereas LMW-HA induces inflammation and is related to the angiogenesis, survival, growth and metastasis of tumors[8]. The accumulation of HA is closely related to the prognosis of patients with malignant tumors, such as malignant breast, prostate, ovarian, and lung tumors[9]. Other factors that are involved in HA metabolism (precursors of HA synthesis, HA synthases, HA receptors, and hyaluronidase) are associated with tumor development[10]. According to previous studies, HA synthases, including HAS1, HAS2 and HAS3, play crucial roles in the process of HA synthesis[11]. CD44 is an important HA receptor. CD44 promotes the metastasis, proliferation and angiogenesis of invasive tumors and accelerates the degradation of HA. Inhibition of CD44 activity induces the apoptosis of invasive tumors[12]. UDP is a precursor required for HA synthesis, and 4-Methylumbelliferone (4-MU), which passes through the blood-brain barrier (BBB), is a competitive precursor inhibitor of UDP[13, 14]. 4-MU exerts antitumor effects on many types of tumors, such as prostate cancer[15], pancreatic cancer[16], and colorectal carcinoma[17]. Based on this evidence, HA and its receptors play important roles in tumor development. However, less is known about the role and molecular mechanisms of abnormal HA accumulation in glioma and further studies are needed. Here, we examined the effect and mechanism of HA metabolism on glioma by interfering with HA metabolism through the suppression of production of the HA precursor, the expression of hyaluronic acid synthase, and the binding of HA with its receptor.

Autophagy is essential for maintaining the growth of tumor cells[18]. HA has a clear relationship with reactive oxygen species (ROS)[19]. ROS and autophagy are closely related. Importantly, ROS are crucial regulators of autophagy under various conditions[20]. HA has been shown to regulate cell survival and growth through the PI3K/AKT/mTOR pathway, which is a typical signaling pathway inducing cell autophagy[21]. Additionally, in patients with osteoarthritis (OA), HA regulates autophagy by altering the miRNA expression profile[22]. These evidences prompted us to explore whether abnormal HA metabolism affects the proliferation of glioma cells by regulating autophagy. Alterations in HA metabolism induced by silencing HAS3, blocking its binding with the receptor CD44 or administering 4-MU inhibited autophagy flux, arrested the cell cycle at G1 phase and subsequently inhibited the proliferation of glioma cells in the present study. In conclusion, interfering with the synthesis of HA or blocking binding to its receptor may be a potential therapy for glioma treatment.

Materials And Methods

Cell culture

Human glioma cell lines (U251 and LN229) were obtained from the China Infrastructure of Cell Line Resource (National Science & Technology Infrastructure, NSTI). The two glioma cell lines were cultured with Dulbecco's Modified Eagle's Medium (DMEM; 10013CVRC, Corning, USA) containing 10% fetal bovine serum (FBS; 16000-044, Gibco, USA) in an incubator at 37°C with a 5% CO2 atmosphere.

MTT assay

Glioma cells were cultured in 96-well dishes (JET BIOFIL, China) at a density of 4000 cells/well. After treating the cells under different conditions, 10 μl of MTT (5 mg/ml) were added to each well, and the cells were cultured for four hours at 37°C in the presence of 5% CO_2. Next, the culture medium was replaced with 150 μl of dimethyl sulfoxide. Cell viability was measured by recording the absorbance at a wavelength of 490 nm using a BioTek ELx800 (USA) microplate reader according to the manufacturer's instructions. MTT (Cat# HY-15924) and chloroquine (Cat# HY-17589A) were purchased from MedChemExpress, and 4-MU (Cat# M1381) was purchased from Sigma-Aldrich. The CD44 antibody (Cat# 217594-100ULCN) was purchased from Millipore.

Cell transfection

The Lipofectamine 2000 reagent (Cat# 11668019, Invitrogen, USA) was used to transfect the glioma cell lines with siRNAs according to the manufacturer's instructions. The siRNAs were purchased from GENERAL BIOSYSTEMS (China). Lentiviruses expressing shNC, shHAS3 and shCD44 were purchased from Wanleibio (China).

Quantitative real-time PCR (qRT-PCR)

Total RNA was extracted using TRIzol reagent (Cat# 15596026, Invitrogen, USA) and reverse transcribed using a Roche Transcriptor cDNA Synthesis Kit (Cat #4897030001) according to the manufacturer's specifications. A SYBR Green PCR Master Mix kit (Cat# 4913914001, Roche, Germany) was utilized to verify the expression of the target gene. qRT-PCR was performed using an ABI Prism 7500 fast thermocycler (Applied Biosystems, CA). The sequences of the GAPDH, HAS3 and CD44 primers are shown in Table 1.

Western blot analysis

Protein samples were extracted from glioma cell lines/glioma tissues. Protein samples were separated on 12.5% SDS-PAGE gels and transferred to polyvinylidene difluoride (PVDF) membranes. The membranes were blocked with 5% skim milk and incubated with the primary antibody at 4°C overnight. On the next day, membranes were incubated with fluorescent-dye conjugated secondary antibodies at room temperature for 2 h. The membranes were observed using a ChemiDoc XRS + Imaging System (Bio-Rad,

USA). The following main antibodies utilized in the present study: P62 (18420-1-AP, Proteintech), LC3 (L7543, Sigma), CCND1 (AF0931, Affinity), CCNB1 (DF6786, Affinity), HAS3 (DF13055, Affinity), CD44 (A0340, Abclonal), and β-actin (TA-09, ZSGB-BIO).

ELISA

An ELISA kit (Cat#10800) was purchased from Shanghai Jianglai Industrial Limited By Share Ltd. Glioma cells or glioma tissues were treated with RIPA lysis buffer on ice. After centrifugation, the supernatants from glioma cells or glioma tissues were obtained. Fifty microliters of supernatant and standard samples were added to each well. Horseradish peroxidase (HRP) (100 μl) was added to each well, and the cells were incubated at 37°C for 1 h. The primary liquid was replaced with a scrubbing solution and dried using absorbent paper by patting the plate 5 times. Substrates A (50 μl) and B (50 μl) were added to each well, and the samples were incubated in the dark for 15 minutes at 37°C. Stop buffer (50 μl) was then added to each well. Finally, the optical density (OD) was measured at a wavelength of 450 nm using a BioTek elx800 (USA) microplate reader according to the manufacturer's instructions.

Transmission electron microscopy (TEM)

Cells immobilized with 2.5% glutaraldehyde at 4°C were postfixed with 1% osmium tetroxide, followed by dehydration in increasing concentrations of ethanol and acetone. Autophagic vesicles were observed using TEM.

GFP-RFP-LC3 fluorescence analysis

U251 glioma cells were transfected with the GFP-RFP-LC3 lentivirus for 24 h. Autophagy flux was observed according to the manufacturer's protocol. After treatment under different conditions, the fluorescence was observed using a confocal microscope, in which yellow dots represented autophagosomes and red dots represented autolysosomes.

Flow cytometry analysis of the cell cycle

Cells were collected and fixed with 70% ethyl alcohol for 24 h. Next, the cells were stained with a cell cycle analysis kit (Beyotime P0010, China) at 4°C for 30 minutes. The cell cycle results were detected using a flow cytometer.

Immunohistochemical (IHC) staining

The tissues were embedded in paraffin, sliced and incubated with primary and secondary antibodies to visualize the target protein under the microscope. The main antibodies utilized in the present study were as follows: HAS3 (BF0681, Affinity), CD44 (A0340, Abclonal), HA (Ab53842, Abcam), and Ki67 (A2094-100, Abclonal).

Mouse tumor model

BALB/C nude mice were purchased from Beijing Vital River Laboratory Animal Technology Co., Ltd. (China). For the subcutaneous tumor model, mice were divided into control and experimental groups. Serum-free DMEM (100 μl) containing 5×10^6 cells was injected subcutaneously at 1 cm. The volume of tumors was measured twice weekly, and the mice were sacrificed 23 days later. The tumor volume was calculated using the formula $(\text{width})^2 \times (\text{length})/2$. For orthotopic transplantation, mice were divided into control and experimental groups. Serum-free DMEM (5 μl) containing 2×10^6 cells was injected into the mouse brain. The injection location was 2.5 mm to the right of the midline and 0.5 mm behind the coronal suture at a depth of 3.5 mm. After 21 days, the two groups were scanned using MRI. At 52 days, the nude mice with residual orthotopic tumors were euthanized. Finally, the survival curve was drawn according to the times of death of the mice. All animal experiments complied with the Institutional Animal Care and Use Committee at Harbin Medical University (No. HMUIRB-2008-06) and the Institute of Laboratory Animal Science of China (A5655-01).

Bioinformatics analysis

TCGA database was used to draw the curve showing the expression of target genes in patients with LGG and GBM. According to TCGA database, we drew the disease-free survival (DFS) curves for target genes in patients with LGG and GBM. Gene expression data for 516 patients with LGG and 154 patients with GBM and DFS data for 476 patients with LGG and 94 patients with GBM were included. The top 75% was chosen for the demarcation point. The data from TCGA were downloaded from https://xenabrowser.net/datapages/?hub=https://tcga.xenahubs.net:443.

Statistical analysis

Statistical analyses comparing data between groups were performed using Student's t-test or one-way ANOVA (Prism software version 7.0). $P < 0.05$ indicated statistical significance (*).

Results

The levels of hyaluronic acid, HAS3 and CD44 are increased and negatively correlated with the prognosis of patients with different grades of glioma.

HA levels were first detected in glioma tissues to investigate whether abnormal HA metabolism is associated with glioma. The level of HA was significantly increased in tissues from patients with different grades of gliomas compared with normal tissues (Fig. 1A and C). Based on the abnormal accumulation of HA in patients with different grades of gliomas, we wondered whether factors related to HA metabolism are associated with glioma growth. HA-related synthases (HAS1, HAS2, and HAS3) and the receptor CD44 play important roles in the synthesis and biological function of HA. Therefore, a bioinformatics analysis was performed to analyze the expression of HA synthases and CD44. The results shown in Supplementary Fig. 1A indicated that HAS1 was negatively correlated with the disease-free survival time of patients with high-grade glioma; however, the correlation was not significant for patients with low-grade glioma (LGG). Additionally, HAS1 was expressed at higher levels in patients with LGG than

in patients with glioblastoma multiforme (GBM). Interestingly, although HAS3 and HAS2 expression were upregulated in patients with GBM compared with patients with LGG, only HAS3 expression was negatively correlated with the disease-free survival time in both patients with LGG and GBM (Supplementary Fig. 1B; Fig. 1D). CD44 is an important receptor for HA. CD44 expression was also upregulated and negatively correlated with the prognosis of both patients with LGG and GBM (Fig. 1E). Therefore, HAS3 and CD44 were chosen for further analysis of HA metabolism in glioma. Additionally, our research confirmed the significantly increased expression levels of HAS3 and CD44 in LGG and GBM tissues compared with normal tissues (Fig. 1B-C). Overall, HA, HAS3 and CD44 levels are significantly increased in glioma tissues and may play important roles in glioma progression.

Interfering with HAS3 and CD44suppresses glioma proliferation in vitro and in vivo.

We next explored the effects of interfering with HA metabolism mediated by inhibiting HAS3 or CD44 on glioma progression. First, HAS3 expression was knocked down in U251 and LN229 glioma cell lines using siRNAs. HA synthesis was inhibited upon HAS3 silencing in U251 and LN229 glioma cell lines (Supplementary Fig 2A). Notably, siRNAs were used to silence HAS3; alternatively, an antibody against CD44 was added to the culture media of glioma cells. The results of the MTT assay showed that the inhibition of HAS3 or treatment with an antibody against CD44 significantly decreased the viability of U251 and LN229 cells (Fig. 2A-B). Exogenous HA reversed this effect of HAS3 knockdown. Nevertheless, the addition of exogenous HA did not reverse the effect of a treatment with the CD44 antibody on glioma cells (Fig. 2C). A potential explanation for this result is that the CD44 antibody inhibits the binding of exogenous HA to its receptor CD44, rather than the synthesis of HA. Moreover, inhibition of HAS3 or treatment with the CD44 antibody decreased the expression of Ki67 in U251 or LN229 glioma cells, respectively (Fig. 2D and Supplementary Fig. 2B). We established stable U251cell lines with knockdown of HAS3 and CD44 to further analyze the effects of HAS3 and CD44 on glioma cell viability and proliferation in vivo. As shown in Supplementary Fig. 2C, HAS3 and CD44 expression were significantly decreased in glioma cells transfected with the HAS3 siRNA and CD44 siRNA, respectively, compared with control glioma cells. A subcutaneous tumor model and an orthotopic tumor model were then established in nude mice using the stable U251cell lines. The inhibition of HAS3 or CD44 in vivo significantly decreased the glioma volumes, extended the survival time of mice and downregulated the expression of Ki67 compared with controls (Fig. 2E-G, Supplementary Fig. 2D-E). As expected, silencing of HAS3 also reduced the production of HA in vivo (Fig. 2E). Overall, the inhibition of HAS3 and CD44 decreased the proliferation of glioma cells both in vitro and in vivo.

Interfering with HAS3 and CD44 blocked autophagy flux in glioma.

According to previous study, HA eliminates ROS. ROS are closely associated with cell autophagy, and HA modulates the activity of the PI3K/AKT/mTOR pathway, which is associated with autophagy. Additionally, HA regulates cell autophagy in patients with OA. According to these findings, we hypothesized that strategies interfering with HA metabolism would affect glioma growth by regulating autophagy. We transfected the HAS3 siRNA or added CD44 antibody to U251 glioma cells to confirm this

hypothesis. Then, the number of autophagic vesicles was quantified using transmission electron microscopy (TEM). HAS3 silencing or a treatment with the CD44 antibody increased the number of autophagic vesicles in glioma cells (Fig. 3A). Western blot results showed increased levels of MAP1LC3B-II and P62 in vitro and in vivo (Fig. 3B-C). The simultaneous increase in LC3 and P62 levels has been reported to indicate the blockade of autophagy flux in cells[23]. GFP-RFP-LC3 fluorescence assays were used to evaluate autophagy flux and confirm the effects of altered HA metabolism on autophagy flux. As expected, HSA3 silencing or the CD44 antibody treatment increased the number and intensity of yellow fluorescent dots in glioma cells compared with cells in the control group (Fig. 3D). This evidence further suggests that autophagy flux is blocked after HAS3 silencing or the binding of HA to CD44 receptors is inhibited in glioma cells. Moreover, exogenous HA reversed the effect of HAS3 silencing on autophagy (Supplementary Fig. 3A). Based on these results, treatments interfering with HA metabolism by silencing HAS3 or the application of an antibody against CD44 blocks autophagy flux.

The blockade of HAS3 and CD44 combined with autophagy inhibitors exert a synergistic inhibitory effect on glioma.

CQ (Chloroquine), an inhibitor of autophagy flux, was used to measure autophagy flux in glioma cells and further confirm that treatments that interfere with HA metabolism inhibit cell proliferation by inhibiting autophagy flux. As shown in Fig. 4A, the Western blot results revealed a further increase levels of the MAP1, LC3B-II, and P62 proteins following the silencing of HAS3 or treatment with the CD44 antibody in cells treated with CQ. HAS3 silencing or treatment with the CD44 antibody combined with CQ exerted a synergistic effect on reducing the viability of glioma cells and levels of the Ki67 protein (Fig. 4B-D and 5A). Cell cycle arrest is essential for cell proliferation. Therefore, we investigated the effect of silencing HAS3 or treatment with CD44 antibodies on glioma cell cycle arrest. The results of the flow cytometry analysis showed that HAS3 silencing or the CD44 antibody treatment caused cells to remain in G1 phase compared with cells in the control group, and the CQ treatment enhanced this effect (Fig. 5B). More importantly, silencing HAS3 or treatment with the anti-CD44 antibodies decreased the levels of the cell cycle-related proteins cyclin B1 and cyclin D1 in glioma cells, and the CQ treatment further enhanced this effect (Fig. 5C). Inhibition of HAS3 or treatment with the CD44 antibody combined with autophagy inhibitors exerted synergistic inhibitory effects on glioma proliferation through a molecular mechanism that involves arresting the cell cycle in G1 phase.

4-MU suppresses glioma proliferation by blocking autophagy flux and further affecting the cell cycle in vitro and in vivo.

UDP is a precursor required for HA synthesis, and 4-MU is a competitive inhibitor of UDP with the ability to penetrate the BBB. In addition, 4-MU inhibited HA synthesis in glioma cells (Supplementary Fig. 3B). Therefore, we examined the effect of 4-MU dissolved in DMSO on glioma cells in vitro and in vivo. As shown in Fig. 6A, 4-MU decreased the viability of U251 and LN229 glioma cells in a dose- and time-dependent manner. Immunofluorescence staining revealed a significant decrease in Ki67 expression in both U251 and LN229 cell lines (Fig. 6B and Supplementary Fig. 3C). Moreover, 4-MU increased the

number of autophagic vesicles in vitro (Fig. 6C) and the levels of the MAP1, LC3B-II, and P62 proteins in vitro and in vivo (Fig. 6D-E). GFP-RFP-LC3 fluorescence assays showed that 4-MU blocked the autophagy flux of glioma cells (Fig. 6F). Exogenous HA reversed these effects of 4-MU on glioma cells (Supplementary Fig. 3D-E). Interestingly, 4-MU combined with CQ also resulted in a synergistic effect on decreasing cell viability and the levels of Ki67, a cell proliferation marker, increasing the levels of the MAP1, LC3B-II, and P62 proteins, which are autophagy markers, increasing the percentage of cells in the G1 phase, and decreasing the levels of cell cycle-related proteins, such as cyclin B1 and cyclin D1 (Fig. 7A-E and Supplementary Fig. 3F). A subcutaneous tumor model and an orthotopic tumor model were established with U251 glioma cells to further verify the effect of 4-MU on glioma cells. As shown in Fig. 7F-H and Supplementary Fig. 3G-H, 4-MU decreased the volume of glioma tissues, and the levels of HA and Ki67 were also decreased. Importantly, mice in the 4-MU treatment group lived longer than mice in the control group. Overall, 4-MU suppressed the proliferation of glioma cells in vitro and in vivo by blocking autophagy flux.

Discussion

Glioma, particularly glioblastoma, is a common malignant tumor that threatens human health because of its high disability and mortality rates, and patients often rapidly progress to death[24, 25]. Although many studies have proposed that the interaction between genes and the external environment leads to the occurrence of glioma, the pathogenesis of glioma remains unclear.

The metabolic remodeling of tumors and the microenvironment are closely related to tumor progression[26, 27]. HA is an important extracellular matrix component in the tumor microenvironment. Previous researchers have confirmed that the abnormal accumulation of HA is related to dysregulated expression of HA synthases and HA degradation enzymes in patients with many pathological conditions, such as cancer, injury and inflammation[28]. In the present study, we focused on HA synthesis and CD44, a specific HA receptor, rather than HA degradation. HA production is catalyzed by three HA synthase (HAS) proteins: HAS1, HAS2 and HAS3. These three key enzymes have different physiological and pathological functions. Some studies have observed a specific HAS expression pattern in different tumor tissues. For example, although HAS3 is expressed at higher levels than HAS2 in metastatic prostate and colon cancer, HAS1 is expressed at low levels in these tumors[8]. This phenomenon may be associated with different cell types and tumor microenvironments. In our study, by analyzing data from The Cancer Genome Atlas (TCGA) database, we observed a negative correlation between HAS1 expression and the disease-free survival time of patients with high-grade glioma, but HAS1 expression was not significantly correlated with the disease-free survival time of patients with LGG. The expression levels of both HAS3 and HAS2 were upregulated in patients with high-grade glioma compared with patients with LGG; however, only HAS3 expression was negatively correlated with the survival time of patients with LGG and high-grade glioma. Therefore, we chose HAS3 for further analysis.

HA is divided into HMW-HA, LMW-HA, and and o-HA. HA synthase (HAS) proteins are associated with high molecular weight HA (HMW-HA). Endoglycosidases (hyaluronidases, HYALs) cleave HA to produce

LMW-HA fragments. Mechanistically, HMW-HA is anchored to the cell surface by CD44 in caveolin-rich lipid rafts and then degraded by HYALs and further internalized and cleaved to produce oligosaccharides[9]. CD44 is a crucial receptor for HA. According to previous studies, HA binds to the CD44 receptor on the cell membrane and participates in tumor differentiation, adhesion, migration and angiogenesis, playing an important role in tumor development[29]. In the present study, treatments interfering with the synthesis of HA, such as 4-MU or HAS3 siRNA, and treatments interfering with the function of the CD44 receptor for HA inhibited the growth of glioma cells in vitro and in vivo. Exogenous HA reversed the inhibition of glioma cell growth caused by HAS3 siRNA and 4-MU in vitro, although exogenous HA did not reverse the effects of blocking CD44. Based on these findings, we speculated that HAS3 promoted the synthesis of HA, followed by an interaction with CD44 to subsequently promote the progression of glioma. In addition, 4-MU inhibited the synthesis of HA, finally leading to a reduction in the binding of HA to CD44.

HA is an important extracellular matrix molecule. In an HA-rich environment, HA promotes cell proliferation and migration. However, the role and mechanism of HA and its metabolism in glioma remain unclear. As shown in the present study, interference with HA metabolism by inhibiting HAS3, CD44 or the precursor of HA synthesis inhibited the proliferation of glioma in vitro and in vivo. The molecular mechanism depends on blocking autophagy flux and further arresting the tumor cell cycle in G1 phase. Autophagy is a mechanism of cellular self-degradation under pressure. Tumor cells obtain amino acids and other macromolecular substances for biosynthesis through autophagy[30]. Autophagy is a double-edged sword that not only promotes the survival of tumor cells but also induces the death of tumor cells, depending on the type of tumor[31]. The data in this study showed that interfering with HA metabolism inhibited autophagy flux and further suppressed glioma proliferation. Moreover, CQ enhanced the inhibition of glioma cell growth induced by interfering with the HA metabolism pathway. Thus, the inhibition of HA metabolism does not completely block autophagy flux. Therefore, CQ and the inhibition of HA metabolism exert a synergistic inhibitory effect on glioma cell growth.

Conclusion

In summary, treatments interfering with HA metabolism inhibit the malignant behavior of glioma cells by blocking autophagy flux. 4-MU functions as a small HA precursor competitive inhibitor with the ability to penetrate the BBB that also exerts an antiglioma effect. Finally, we propose that treatments interfering with HA metabolism and 4-MU may represent effective strategies for glioma treatment in the future.

Abbreviations

HA: Hyaluronic acid

TCGA: The Cancer Genome Atlas

4-MU: 4-Methylumbelliferone

HAS: HA synthase

HAS3: Hyaluronic acid synthase 3

BBB: Blood-brain barrier

HMW-HA: High molecular weight HA

LMW-HA: Low molecular weight HA

o-HA: oligosaccharides

ROS: Reactive oxygen species

OA: osteoarthritis

DFS: Disease-free survival

LGG: low-grade glioma

GBM: glioblastoma multiforme

CQ: Chloroquine

CCND1: Cyclin D1

CCNB1: Cyclin B1

Declarations

Ethics approval and consent to participate

This research was carried out in according to the Ethics Committee of Harbin Medical University Hospital and with the Declaration of Helsinki. All the participants gave written informed consent. All animal experiments complied with the Institutional Animal Care and Use Committee at Harbin Medical University (No. HMUIRB-2008-06) and the Institute of Laboratory Animal Science of China (A5655-01).

Consent for publication

All authors have read and approved of its submission to this journal.

Competing interests

The authors declare that they haven’t potential conflicts of interest.

Availability of data and materials

To the extent reasonable, the dateses used in this research could be provided by corresponding author.

Funding

This research was supported by National Natural Science Foundation of China (NO.81672486, 81972363 and 82002634).

Acknowledgements

We would like to express our sincere thanks to all reviewers and editors for their valuable comments on this study

Authors' contributions

Tao Yan, Penglei Yao, Hua Zhan, Ning Wang: Conceptualization, writing, Project administration, Methodology, Resources. Kaikai Wang, He Yang, Jingxian Sun, Yu Dong, Xin Chen, Enzhou Lu: Data curation, Investigation and Formal analysis, Visualization. Zhixing Zheng, Ruotian Zhang, Xiaoxiong Wang, Ming Gao, Junyi Ye, Xinzhuang Wang: Investigation, Writing - review & editing, Software. Lei Teng, Huailei Liu, Guangshi Zhao: Conceptualization, Funding acquisition, Supervision.

References

1.S. Bastola, M. S. Pavlyukov, D. Yamashita, S. Ghosh, H. Cho, N. Kagaya,I. Nakano. Glioma-initiating cells at tumor edge gain signals from tumor core cells to promote their malignancy. Nat Commun. 2020; 11: 4660.

2.D. Hanahan, L. M. Coussens. Accessories to the crime: functions of cells recruited to the tumor microenvironment. Cancer Cell. 2012; 21: 309-322.

3.C. Roma-Rodrigues, R. Mendes, P. V. Baptista, A. R. Fernandes. Targeting Tumor Microenvironment for Cancer Therapy. Int J Mol Sci. 2019; 20:

4.Ina Sevic, Fiorella Mercedes Spinelli, María José Cantero, Andrea Reszegi, Ilona Kovalszky, Mariana Gabriela García, Laura Alaniz. The Role of the Tumor Microenvironment in the Development and Progression of Hepatocellular Carcinoma. 2019; 29-45.

5.P. Heldin, K. Basu, B. Olofsson, H. Porsch, I. Kozlova, K. Kahata. Deregulation of hyaluronan synthesis, degradation and binding promotes breast cancer. J Biochem. 2013; 154: 395-408.

6.R. H. Tammi, A. Kultti, V. M. Kosma, R. Pirinen, P. Auvinen, M. I. Tammi. Hyaluronan in human tumors: pathobiological and prognostic messages from cell-associated and stromal hyaluronan. Semin Cancer Biol. 2008; 18: 288-295.

7.Marco P. Carvalho, Elisabete C. Costa, Sónia P. Miguel, Ilídio J. Correia. Tumor spheroid assembly on hyaluronic acid-based structures: A review. Carbohydrate Polymers. 2016; 150: 139-148.

8.N. Nagy, H. F. Kuipers, A. R. Frymoyer, H. D. Ishak, J. B. Bollyky, T. N. Wight, P. L. Bollyky. 4-methylumbelliferone treatment and hyaluronan inhibition as a therapeutic strategy in inflammation, autoimmunity, and cancer. Front Immunol. 2015; 6: 123.

9.Theerawut Chanmee, Pawared Ontong, Naoki Itano. Hyaluronan: A modulator of the tumor microenvironment. Cancer Letters. 2016; 375: 20-30.

10.Vinata B. Lokeshwar, Summan Mirza, Andre Jordan. Targeting Hyaluronic Acid Family for Cancer Chemoprevention and Therapy. 2014; 123: 35-65.

11.Davide Vigetti, Alberto Passi. Hyaluronan Synthases Posttranslational Regulation in Cancer. 2014; 123: 95-119.

12.F. M. Spinelli, D. L. Vitale, G. Demarchi, C. Cristina, L. Alaniz. The immunological effect of hyaluronan in tumor angiogenesis. Clin Transl Immunology. 2015; 4: e52.

13.T. J. Yates, L. E. Lopez, S. D. Lokeshwar, N. Ortiz, G. Kallifatidis, A. Jordan,V. B. Lokeshwar. Dietary supplement 4-methylumbelliferone: an effective chemopreventive and therapeutic agent for prostate cancer. J Natl Cancer Inst. 2015; 107:

14.A. M. Mueller, B. H. Yoon, S. A. Sadiq. Inhibition of hyaluronan synthesis protects against central nervous system (CNS) autoimmunity and increases CXCL12 expression in the inflamed CNS. J Biol Chem. 2014; 289: 22888-22899.

15.V. B. Lokeshwar, L. E. Lopez, D. Munoz, A. Chi, S. P. Shirodkar, S. D. Lokeshwar,N. Altman. Antitumor activity of hyaluronic acid synthesis inhibitor 4-methylumbelliferone in prostate cancer cells. Cancer Res. 2010; 70: 2613-2623.

16.H. Nagase, D. Kudo, A. Suto, E. Yoshida, S. Suto, M. Negishi,K. Hakamada. 4-Methylumbelliferone Suppresses Hyaluronan Synthesis and Tumor Progression in SCID Mice Intra-abdominally Inoculated With Pancreatic Cancer Cells. Pancreas. 2017; 46: 190-197.

17.Hiroyuki Cho, Seiji Matsumoto, Yoshiko Fujita, Ayumi Kuroda, Toshi Menju, Makoto Sonobe,Seiki Hasegawa. Trametinib plus 4-Methylumbelliferone Exhibits Antitumor Effects by ERK Blockade and CD44 Downregulation and Affects PD-1 and PD-L1 in Malignant Pleural Mesothelioma. Journal of Thoracic Oncology. 2017; 12: 477-490.

18.Alec C. Kimmelman, Eileen White. Autophagy and Tumor Metabolism. Cell Metabolism. 2017; 25: 1037-1043.

19.D. Jiang, J. Liang, P. W. Noble. Hyaluronan as an immune regulator in human diseases. Physiol Rev. 2011; 91: 221-264.

20.X. Zhang, L. Yu, H. Xu. Lysosome calcium in ROS regulation of autophagy. Autophagy. 2016; 12: 1954-1955.

21.Zoe Price, Noor Lokman, Carmela Ricciardelli. Differing Roles of Hyaluronan Molecular Weight on Cancer Cell Behavior and Chemotherapy Resistance. Cancers. 2018; 10: 482.

22.Ji-Feng Xu, Shui-Jun Zhang, Chen Zhao, Bin-Song Qiu, Hai-Feng Gu, Jian-Fei Hong,Ya-Ping Wang. Altered microRNA Expression Profile in Synovial Fluid from Patients with Knee Osteoarthritis with Treatment of Hyaluronic Acid. Molecular Diagnosis & Therapy. 2015; 19: 299-308.

23.W. Yue, A. Hamai, G. Tonelli, C. Bauvy, V. Nicolas, H. Tharinger,M. Mehrpour. Inhibition of the autophagic flux by salinomycin in breast cancer stem-like/progenitor cells interferes with their maintenance. Autophagy. 2013; 9: 714-729.

24.Q. T. Ostrom, H. Gittleman, J. Fulop, M. Liu, R. Blanda, C. Kromer,J. S. Barnholtz-Sloan. CBTRUS Statistical Report: Primary Brain and Central Nervous System Tumors Diagnosed in the United States in 2008-2012. Neuro Oncol. 2015; 17 Suppl 4: iv1-iv62.

25.R. Stupp, W. P. Mason, M. J. van den Bent, M. Weller, B. Fisher, M. J. Taphoorn,Group National Cancer Institute of Canada Clinical Trials. Radiotherapy plus concomitant and adjuvant temozolomide for glioblastoma. N Engl J Med. 2005; 352: 987-996.

26.J. Bi, S. Chowdhry, S. Wu, W. Zhang, K. Masui, P. S. Mischel. Altered cellular metabolism in gliomas - an emerging landscape of actionable co-dependency targets. Nat Rev Cancer. 2020; 20: 57-70.

27.H. H. Lin, Y. Chung, C. T. Cheng, C. Ouyang, Y. Fu, C. Y. Kuo,D. K. Ann. Autophagic reliance promotes metabolic reprogramming in oncogenic KRAS-driven tumorigenesis. Autophagy. 2018; 14: 1481-1498.

28.Jiurong Liang, Dianhua Jiang, Paul W. Noble. Hyaluronan as a therapeutic target in human diseases. Advanced Drug Delivery Reviews. 2016; 97: 186-203.

29.Véronique Orian-Rousseau, Jonathan Sleeman. CD44 is a Multidomain Signaling Platform that Integrates Extracellular Matrix Cues with Growth Factor and Cytokine Signals. 2014; 123: 231-254.

30.M. Long, T. G. McWilliams. Monitoring autophagy in cancer: From bench to bedside. Semin Cancer Biol. 2019;

31.S. Talukdar, A. K. Pradhan, P. Bhoopathi, X. N. Shen, L. A. August, J. J. Windle,P. B. Fisher. MDA-9/Syntenin regulates protective autophagy in anoikis-resistant glioma stem cells. Proc Natl Acad Sci U S A. 2018; 115: 5768-5773.

Tables

Due to technical limitations, table 1 is only available as a download in the Supplemental Files section.

Figures

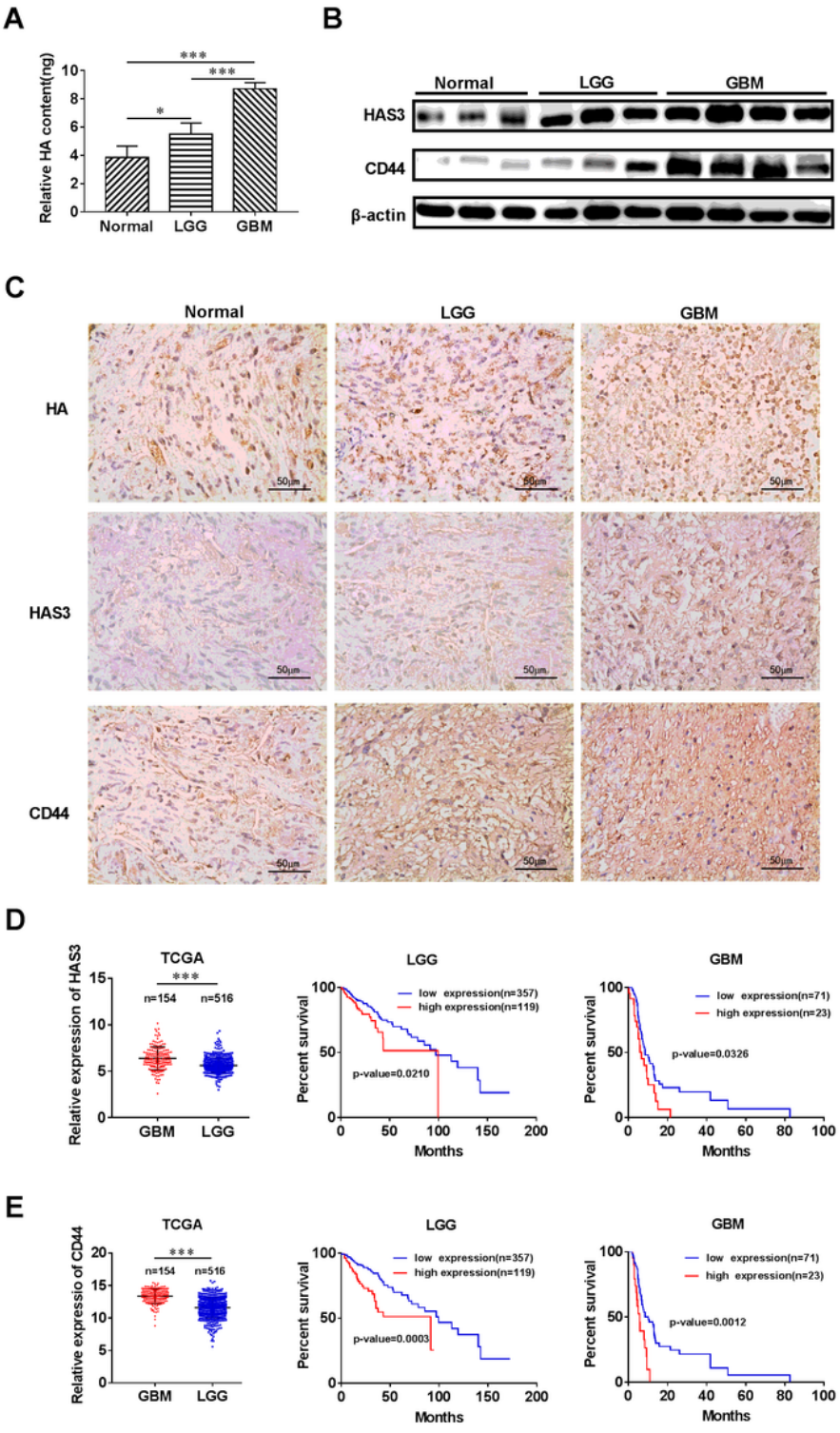

Figure 1

The levels of hyaluronic acid, HAS3 and CD44 are increased and negatively correlated with the prognosis of patients with different grades of glioma. (A) Relative HA content in human glioma tissues of different grades and normal brain tissues. (B) Relative levels of the HAS3 and CD44 proteins in human glioma tissues of different grades and normal brain tissues. (C) Representative images of IHC staining for HA, HAS3 and CD44 in human glioma tissues of different grades and normal brain tissues. Scale bar: 50 μm. (D-E) Relative expression of the HAS3 and CD44 mRNAs in patients with LGG and GBM from TCGA. Survival curves of HAS3 and CD44 for patients with LGG and GBM from TCGA database. Data are presented as means ± SD; *P < 0.05, **P < 0.01, and ***P < 0.001.

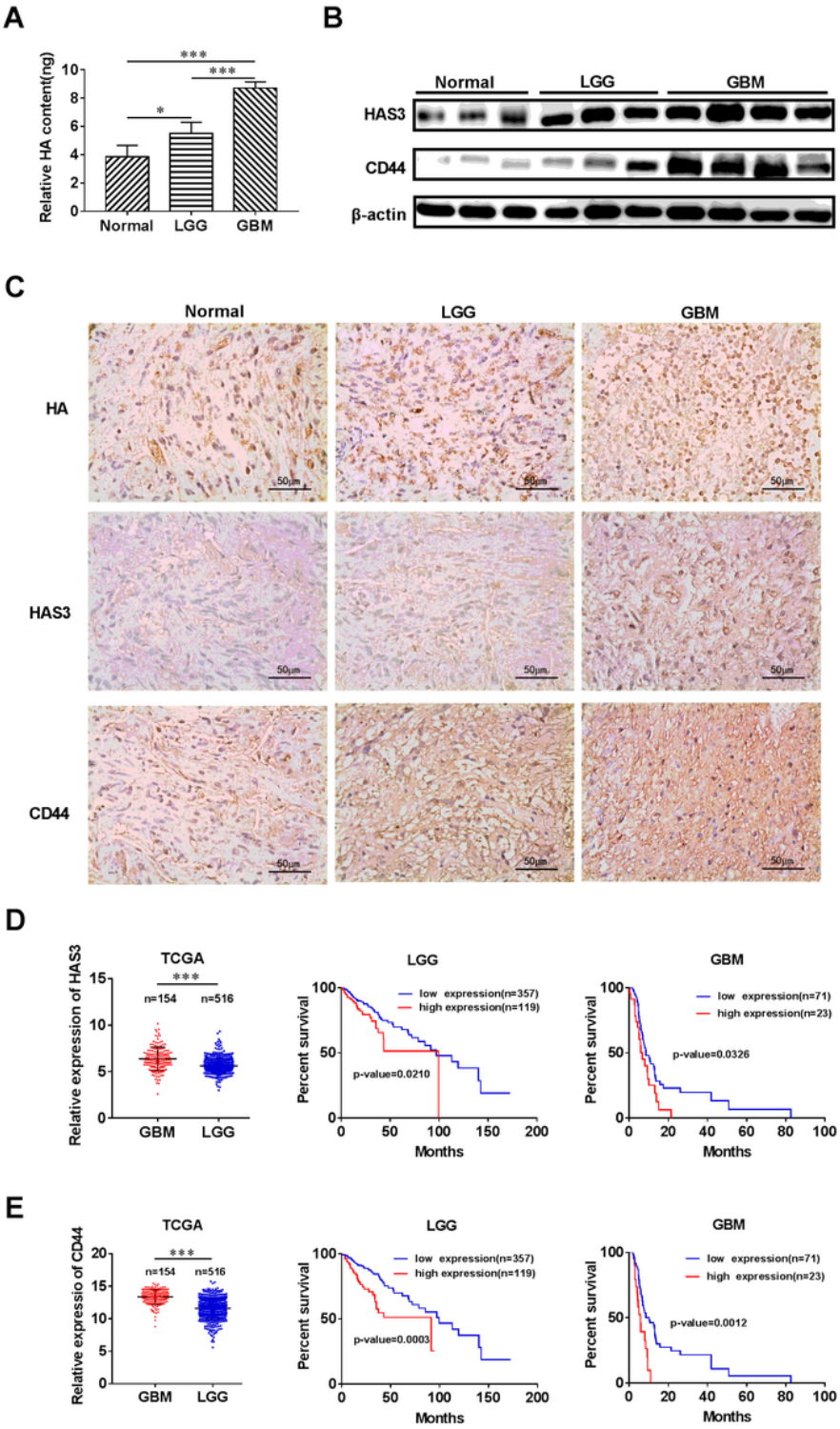

Figure 1

The levels of hyaluronic acid, HAS3 and CD44 are increased and negatively correlated with the prognosis of patients with different grades of glioma. (A) Relative HA content in human glioma tissues of different grades and normal brain tissues. (B) Relative levels of the HAS3 and CD44 proteins in human glioma tissues of different grades and normal brain tissues. (C) Representative images of IHC staining for HA, HAS3 and CD44 in human glioma tissues of different grades and normal brain tissues. Scale bar: 50 μm.

(D-E) Relative expression of the HAS3 and CD44 mRNAs in patients with LGG and GBM from TCGA. Survival curves of HAS3 and CD44 for patients with LGG and GBM from TCGA database. Data are presented as means ± SD; *P < 0.05, **P < 0.01, and ***P < 0.001.

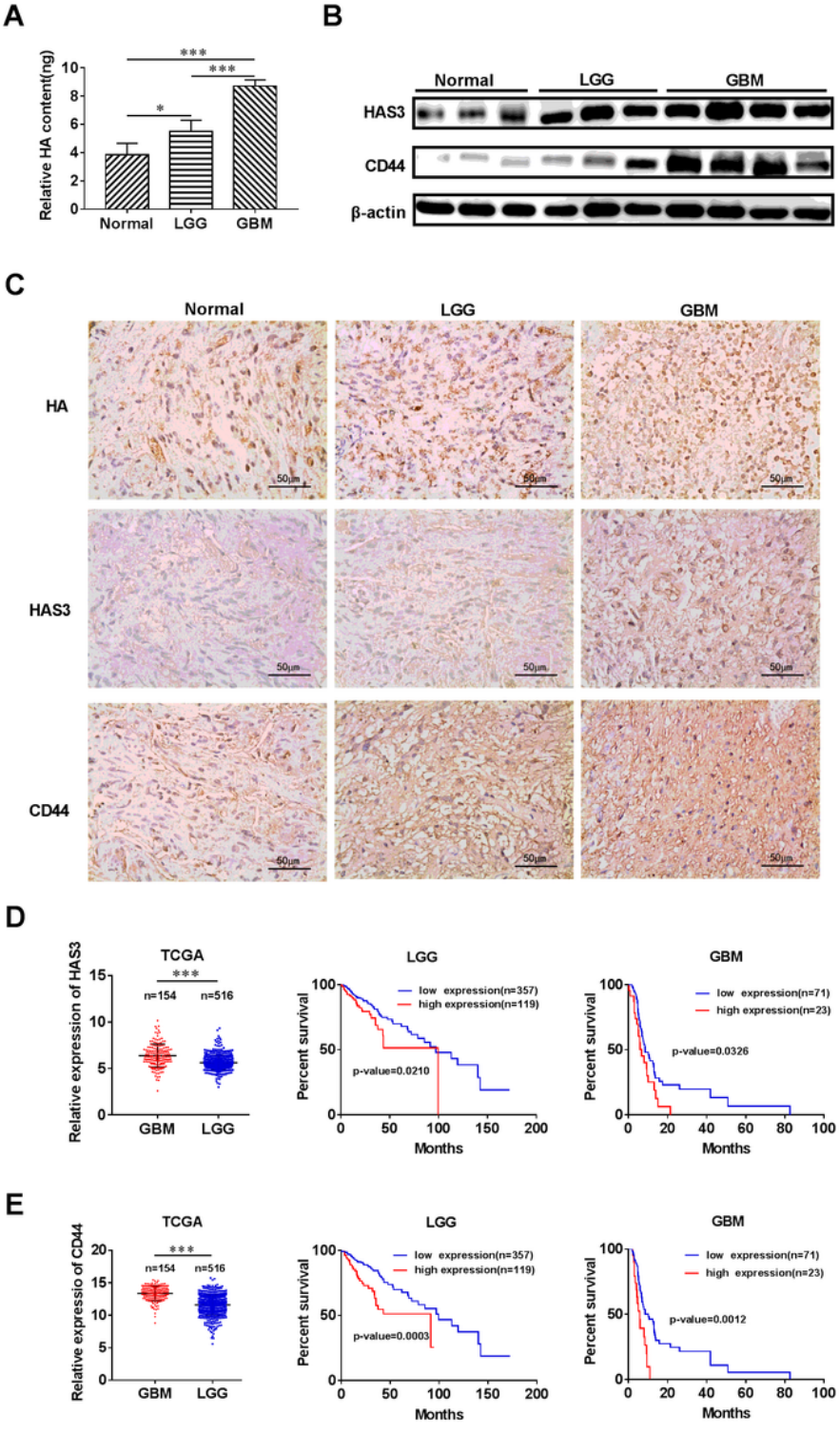

Figure 1

The levels of hyaluronic acid, HAS3 and CD44 are increased and negatively correlated with the prognosis of patients with different grades of glioma. (A) Relative HA content in human glioma tissues of different

grades and normal brain tissues. (B) Relative levels of the HAS3 and CD44 proteins in human glioma tissues of different grades and normal brain tissues. (C) Representative images of IHC staining for HA, HAS3 and CD44 in human glioma tissues of different grades and normal brain tissues. Scale bar: 50 μm. (D-E) Relative expression of the HAS3 and CD44 mRNAs in patients with LGG and GBM from TCGA. Survival curves of HAS3 and CD44 for patients with LGG and GBM from TCGA database. Data are presented as means ± SD; *P < 0.05, **P < 0.01, and ***P < 0.001.

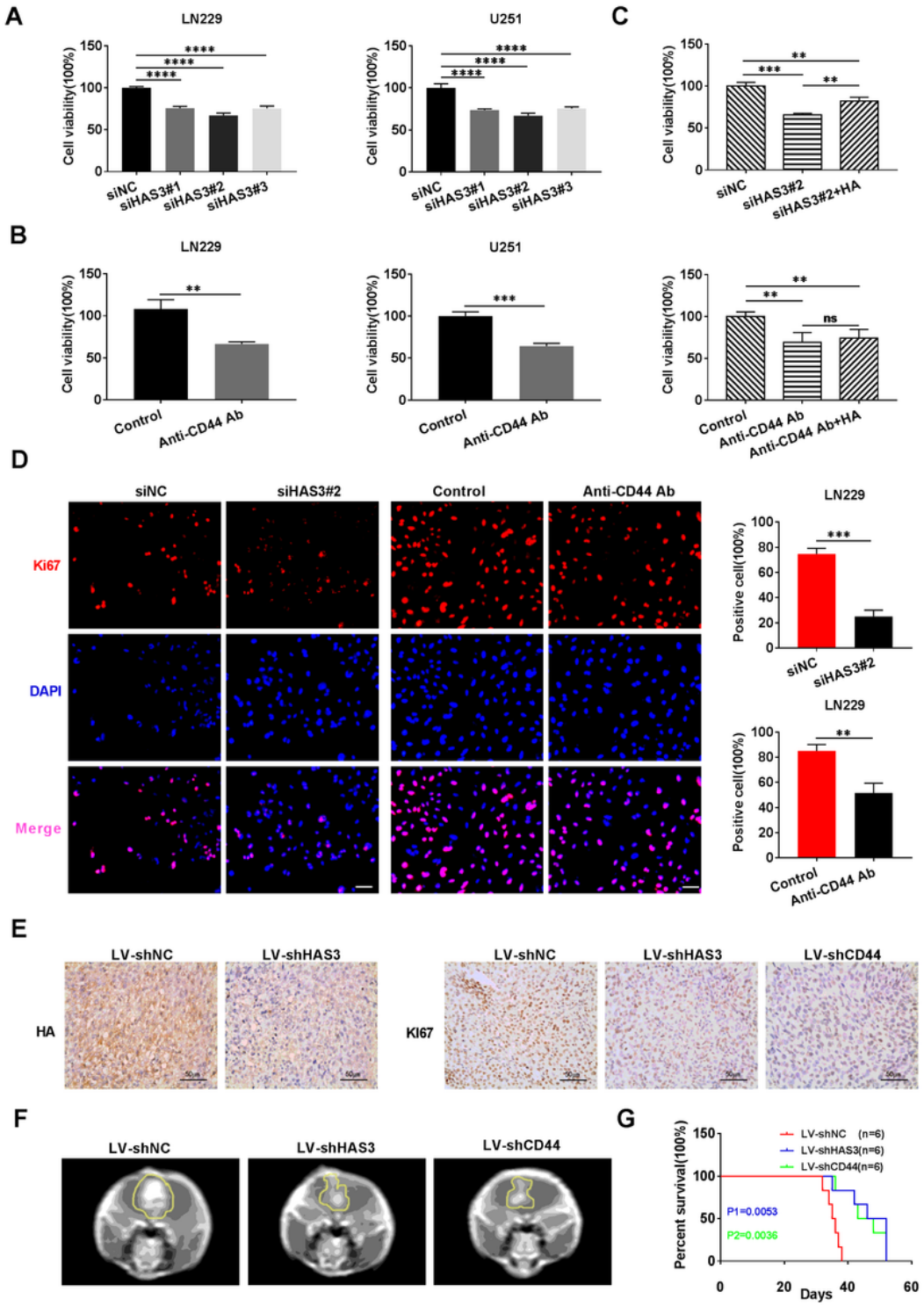

Figure 2

Treatments interfering with HAS3 and CD44 suppress glioma cell proliferation in vitro and in vivo. (A-B) Viability of U251 and LN229 glioma cells transfected with the HAS3 siRNA or treated with CD44 antibody for 48 h. (C) Viability of U251 glioma cells transfected with the HAS3 siRNA or cultured with the CD44 antibody, followed by treatment with HA (25 μg/ml) for 48 h. (D) Levels of the Ki67 protein in LN229 glioma cells were detected using immunofluorescence staining after transfection with the HAS3 siRNA or treatment with the CD44 antibody for 48 h. Scale bar: 50 μm. (E) Representative images of IHC staining for HA in the orthotopic xenograft tumors from the control and lentivirus HAS3 siRNA stably transfected glioma cell groups. Representative images of IHC staining for Ki67 in orthotopic xenograft tumors from the control and lentivirus HAS3 siRNA or lentivirus CD44 siRNA stable transfection glioma cell groups. Scale bar: 50 μm. (F-G) Representative MRI of orthotopic xenograft tumors and survival curves of the control and lentivirus HAS3 shRNA or lentivirus CD44 shRNA stably transfected glioma cell groups. P1: P-value for the comparison of shNC and shHAS3, P2: P-value for the comparison of shNC with shCD44. LV-shNC: negative control lentivirus, LV-shHAS3: HAS3 knockdown lentivirus. LV- shCD44: CD44 knockdown lentivirus. Data are presented as means ± SD; *P < 0.05, **P < 0.01, and ***P < 0.001.

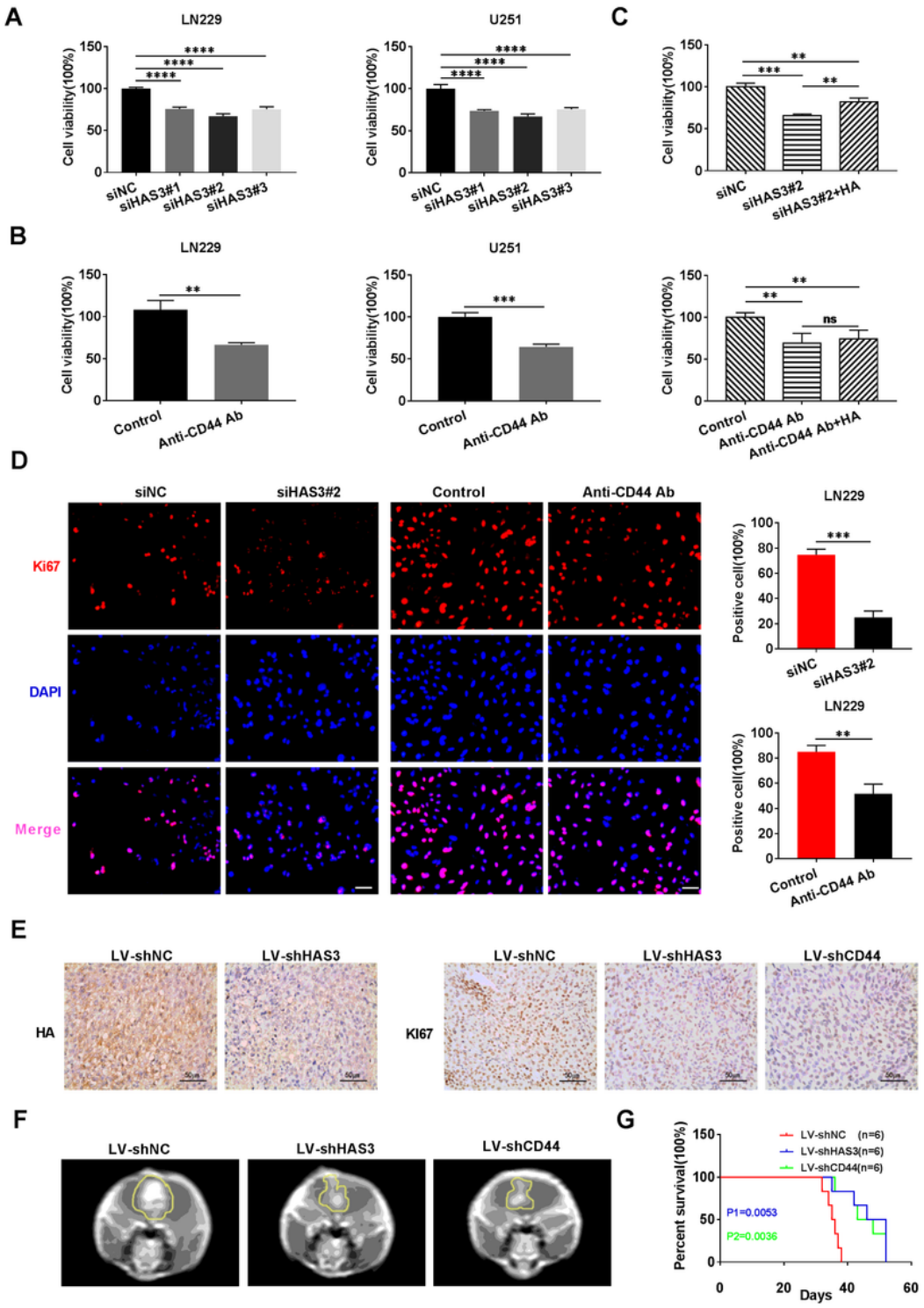

Figure 2

Treatments interfering with HAS3 and CD44 suppress glioma cell proliferation in vitro and in vivo. (A-B) Viability of U251 and LN229 glioma cells transfected with the HAS3 siRNA or treated with CD44 antibody for 48 h. (C) Viability of U251 glioma cells transfected with the HAS3 siRNA or cultured with the CD44 antibody, followed by treatment with HA (25 μg/ml) for 48 h. (D) Levels of the Ki67 protein in LN229 glioma cells were detected using immunofluorescence staining after transfection with the HAS3 siRNA or

treatment with the CD44 antibody for 48 h. Scale bar: 50 μm. (E) Representative images of IHC staining for HA in the orthotopic xenograft tumors from the control and lentivirus HAS3 siRNA stably transfected glioma cell groups. Representative images of IHC staining for Ki67 in orthotopic xenograft tumors from the control and lentivirus HAS3 siRNA or lentivirus CD44 siRNA stable transfection glioma cell groups. Scale bar: 50 μm. (F-G) Representative MRI of orthotopic xenograft tumors and survival curves of the control and lentivirus HAS3 shRNA or lentivirus CD44 shRNA stably transfected glioma cell groups. P1: P-value for the comparison of shNC and shHAS3, P2: P-value for the comparison of shNC with shCD44. LV-shNC: negative control lentivirus, LV-shHAS3: HAS3 knockdown lentivirus. LV- shCD44: CD44 knockdown lentivirus. Data are presented as means ± SD; *P < 0.05, **P < 0.01, and ***P < 0.001.

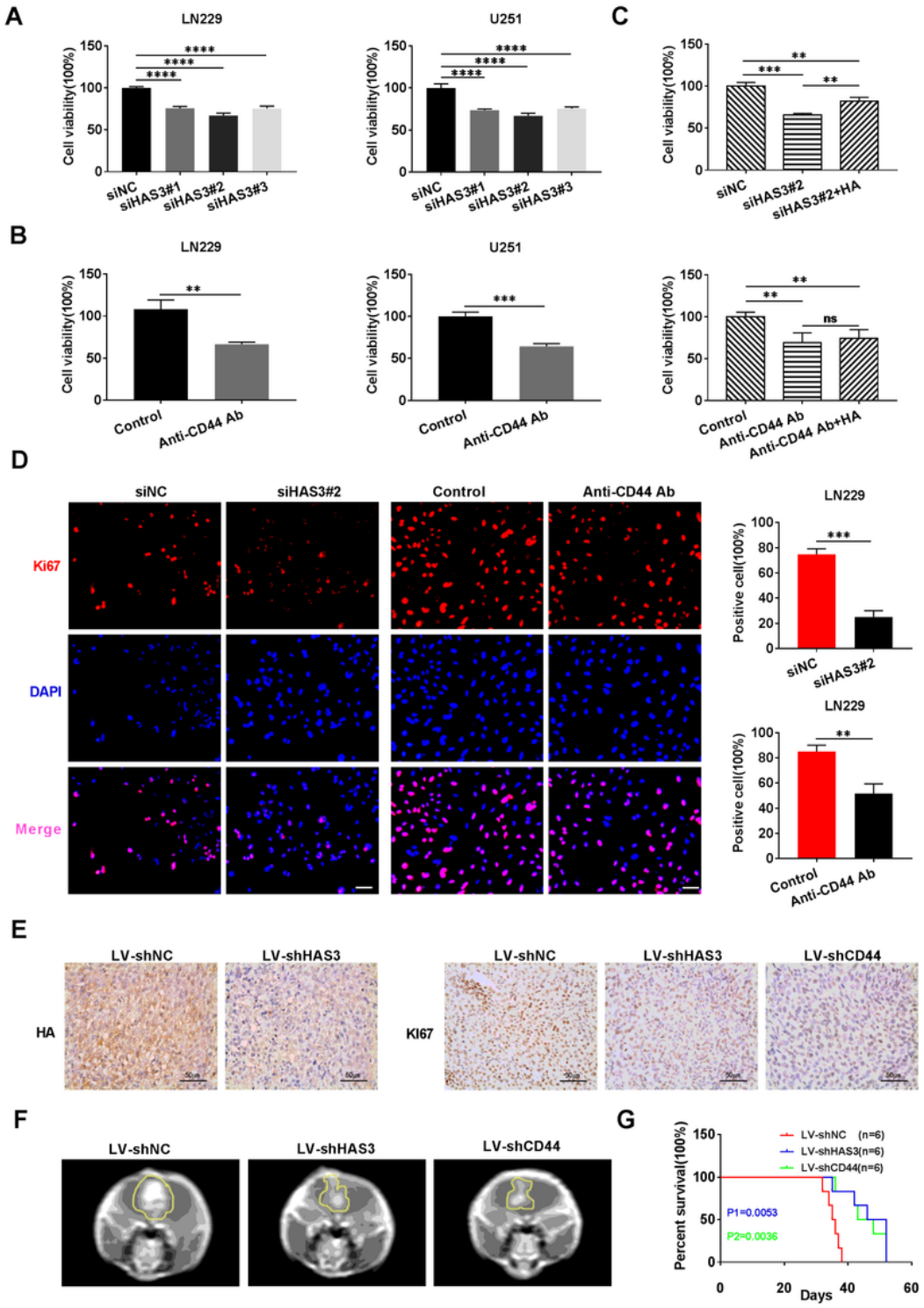

Figure 2

Treatments interfering with HAS3 and CD44 suppress glioma cell proliferation in vitro and in vivo. (A-B) Viability of U251 and LN229 glioma cells transfected with the HAS3 siRNA or treated with CD44 antibody for 48 h. (C) Viability of U251 glioma cells transfected with the HAS3 siRNA or cultured with the CD44 antibody, followed by treatment with HA (25 μg/ml) for 48 h. (D) Levels of the Ki67 protein in LN229 glioma cells were detected using immunofluorescence staining after transfection with the HAS3 siRNA or

treatment with the CD44 antibody for 48 h. Scale bar: 50 μm. (E) Representative images of IHC staining for HA in the orthotopic xenograft tumors from the control and lentivirus HAS3 siRNA stably transfected glioma cell groups. Representative images of IHC staining for Ki67 in orthotopic xenograft tumors from the control and lentivirus HAS3 siRNA or lentivirus CD44 siRNA stable transfection glioma cell groups. Scale bar: 50 μm. (F-G) Representative MRI of orthotopic xenograft tumors and survival curves of the control and lentivirus HAS3 shRNA or lentivirus CD44 shRNA stably transfected glioma cell groups. P1: P-value for the comparison of shNC and shHAS3, P2: P-value for the comparison of shNC with shCD44. LV-shNC: negative control lentivirus, LV-shHAS3: HAS3 knockdown lentivirus. LV- shCD44: CD44 knockdown lentivirus. Data are presented as means ± SD; *P < 0.05, **P < 0.01, and ***P < 0.001.

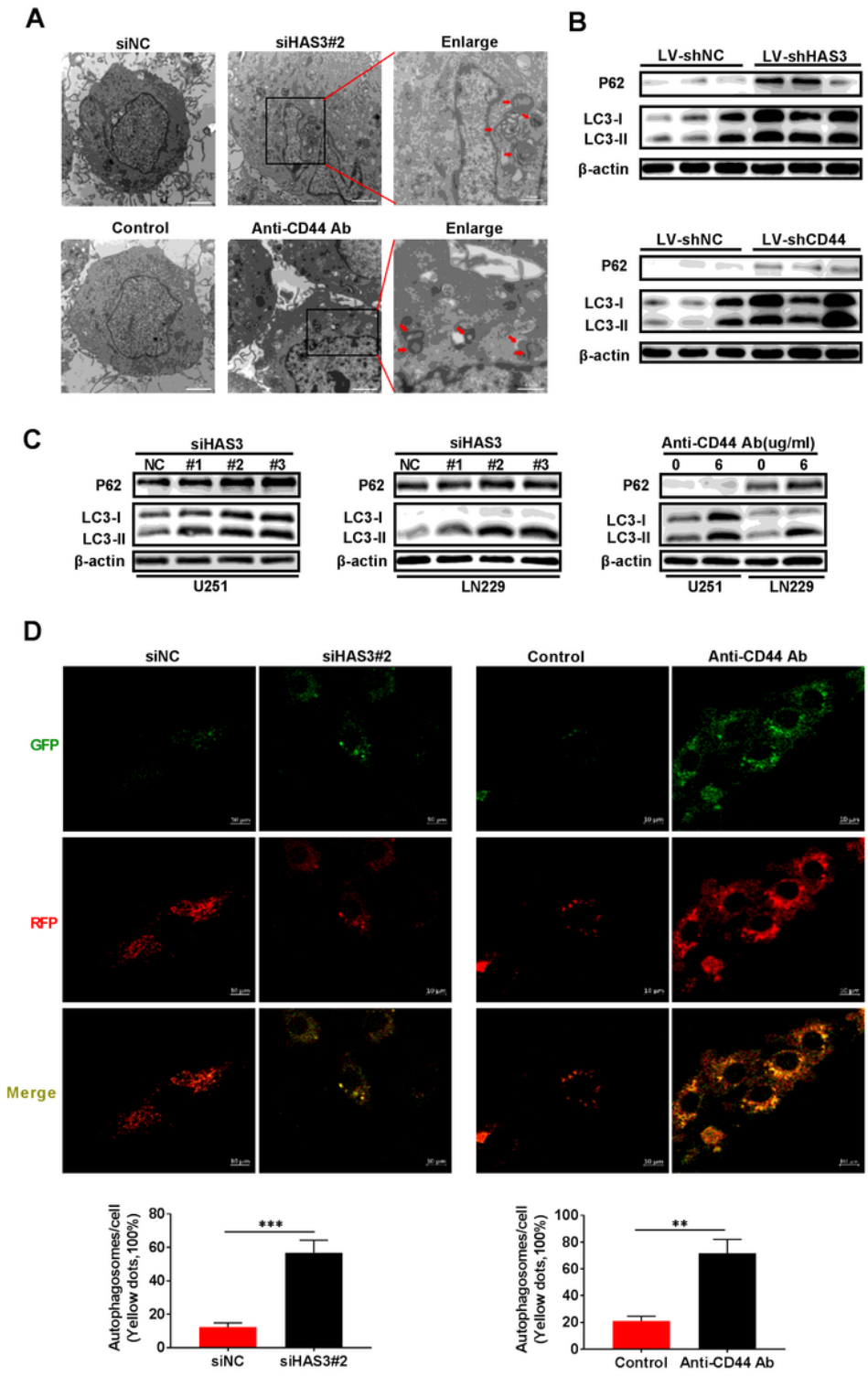

Figure 3

Treatments interfering with HAS3 and CD44 block autophagy flux in vitro and in vivo. (A)TEM images of U251 glioma cells transfected with the HAS3 siRNA or treated with the CD44 antibody for 48 h. The scale bars represent 2 μm in the original image, and the scale bars represent 0.8 μm in the enlarged image. (B) Relative levels of the P62 and LC3 proteins in the orthotopic xenograft tumors from the control and lentivirus HAS3 shRNA or lentivirus CD44 shRNA stably transfected glioma cell groups. (C) Relative levels

of the P62 and LC3 proteins in U251 and LN229 glioma cells transfected with the HAS3 siRNA or treated with the CD44 antibody for 48 h. (D) Results of the GFP-RFP-LC3 fluorescence assay using U251 glioma cells transfected with the HAS3 siRNA or treated with the CD44 antibody for 48 h. Scale bar: 10 μm. Data are presented as means ± SD; *P < 0.05, **P < 0.01, and ***P < 0.001.

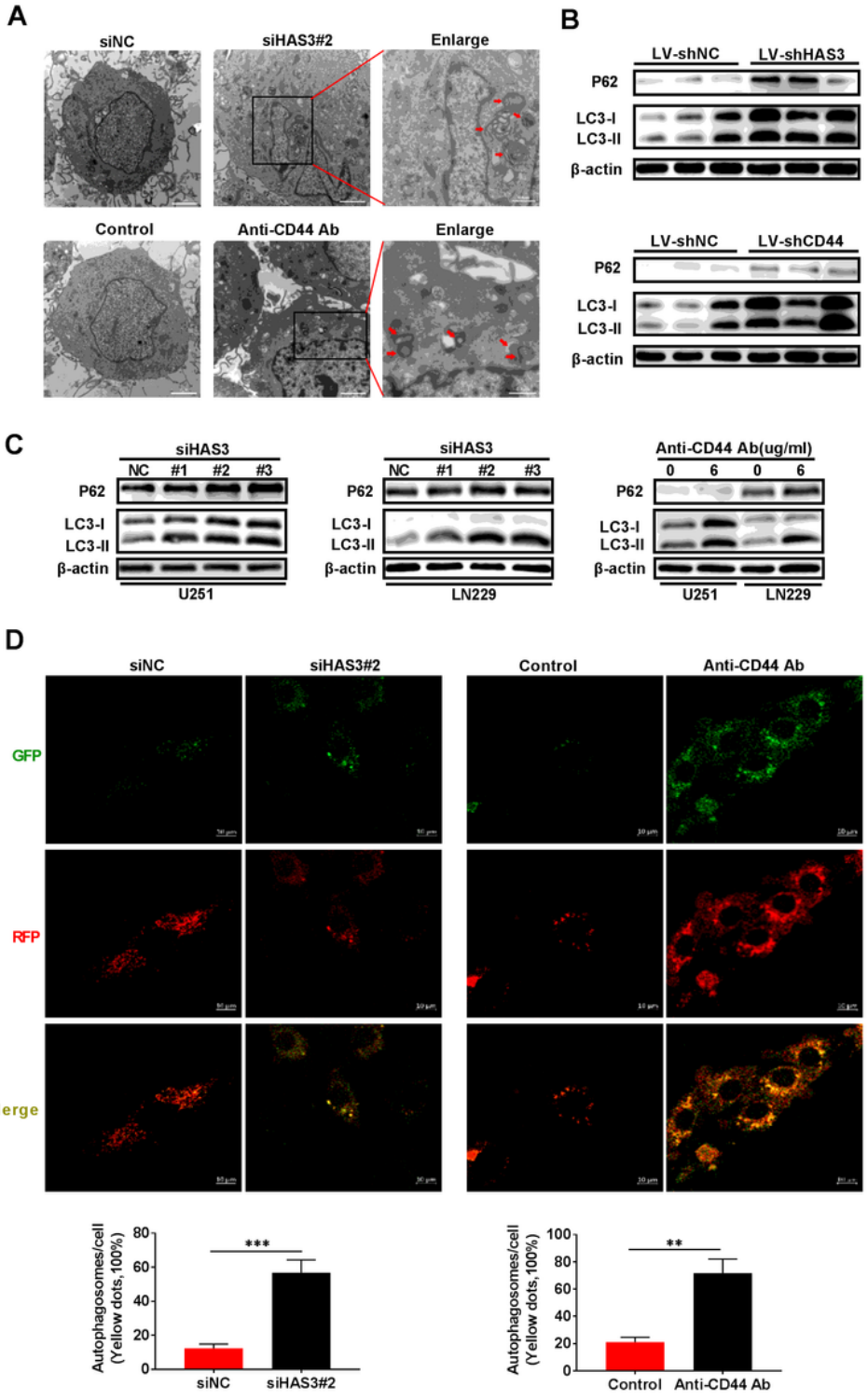

Figure 3

Treatments interfering with HAS3 and CD44 block autophagy flux in vitro and in vivo. (A)TEM images of U251 glioma cells transfected with the HAS3 siRNA or treated with the CD44 antibody for 48 h. The scale bars represent 2 μm in the original image, and the scale bars represent 0.8 μm in the enlarged image. (B) Relative levels of the P62 and LC3 proteins in the orthotopic xenograft tumors from the control and lentivirus HAS3 shRNA or lentivirus CD44 shRNA stably transfected glioma cell groups. (C) Relative levels of the P62 and LC3 proteins in U251 and LN229 glioma cells transfected with the HAS3 siRNA or treated with the CD44 antibody for 48 h. (D) Results of the GFP-RFP-LC3 fluorescence assay using U251 glioma cells transfected with the HAS3 siRNA or treated with the CD44 antibody for 48 h. Scale bar: 10 μm. Data are presented as means ± SD; *P < 0.05, **P < 0.01, and ***P < 0.001.

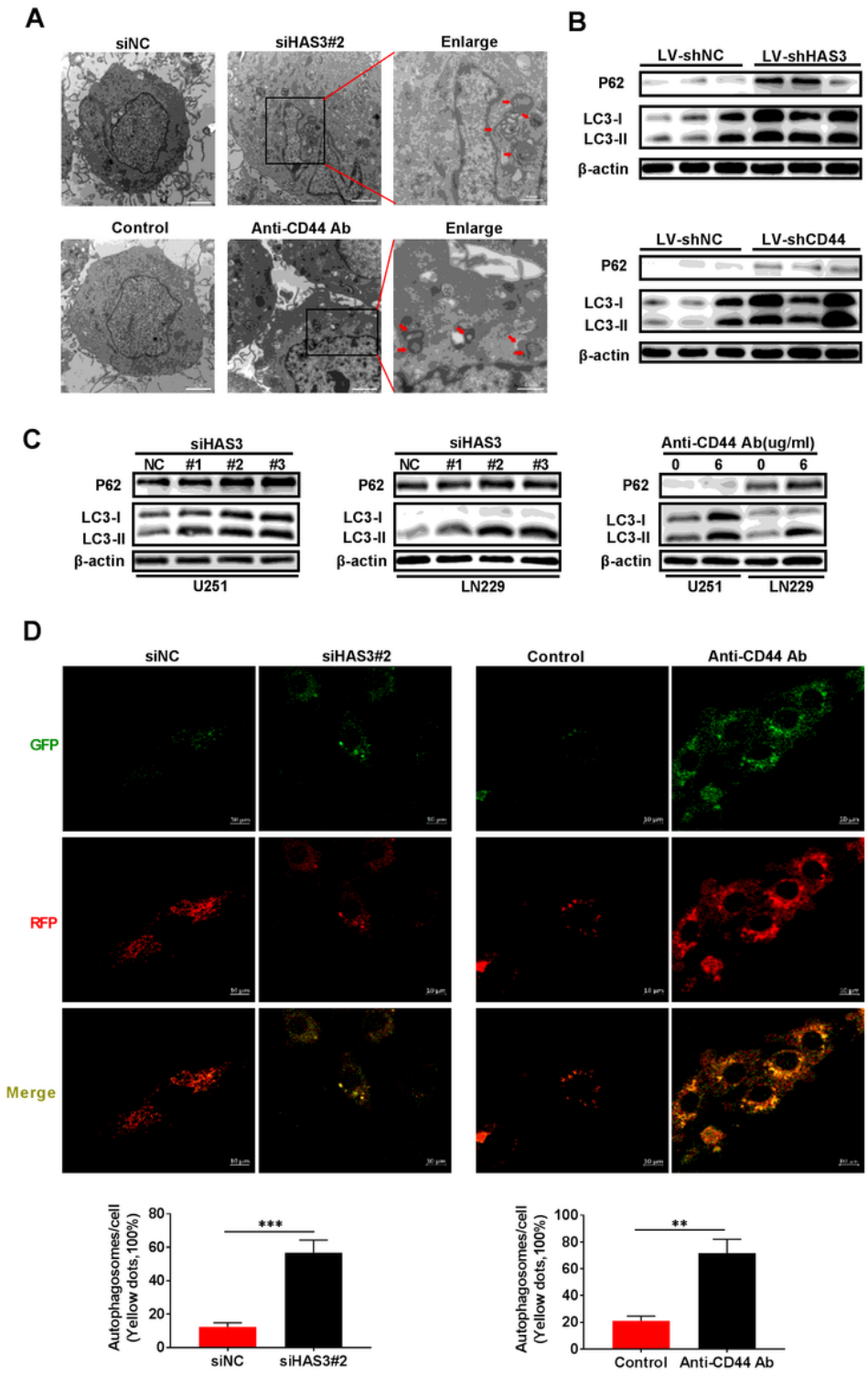

Figure 3

Treatments interfering with HAS3 and CD44 block autophagy flux in vitro and in vivo. (A)TEM images of U251 glioma cells transfected with the HAS3 siRNA or treated with the CD44 antibody for 48 h. The scale bars represent 2 μm in the original image, and the scale bars represent 0.8 μm in the enlarged image. (B) Relative levels of the P62 and LC3 proteins in the orthotopic xenograft tumors from the control and lentivirus HAS3 shRNA or lentivirus CD44 shRNA stably transfected glioma cell groups. (C) Relative levels

of the P62 and LC3 proteins in U251 and LN229 glioma cells transfected with the HAS3 siRNA or treated with the CD44 antibody for 48 h. (D) Results of the GFP-RFP-LC3 fluorescence assay using U251 glioma cells transfected with the HAS3 siRNA or treated with the CD44 antibody for 48 h. Scale bar: 10 μm. Data are presented as means ± SD; *P < 0.05, **P < 0.01, and ***P < 0.001.

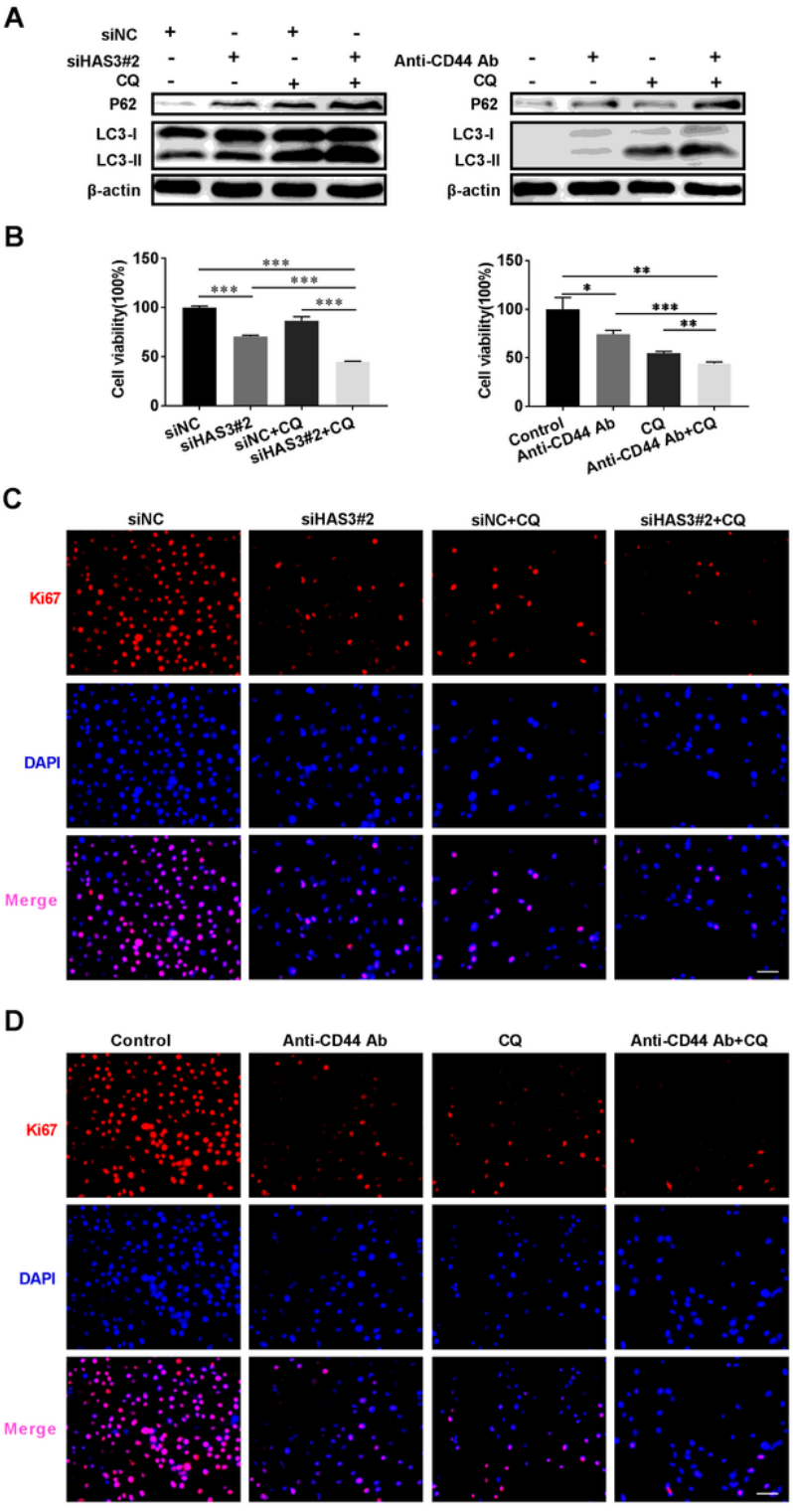

Figure 4

Treatments interfering with HAS3 and CD44 combined with autophagy inhibitors exert synergistic effects on glioma cell viability and autophagy levels. (A) Relative levels of the P62 and LC3 proteins in U251 glioma cells transfected with the HAS3 siRNA or cultured with the CD44 antibody, followed by treatment with CQ (30 mmol/L) for 48 h. (B) Viability of U251 glioma cells transfected with the HAS3 siRNA or cultured with the CD44 antibody, followed by treatment with CQ (30 mmol/L) for 48 h. (C-D) Levels of the Ki67 protein in U251 glioma cells were detected using immunofluorescence staining after transfection with the HAS3 siRNA or culture with CD44 antibody, followed by treatment with CQ (30 mmol/L) for 48 h. Scale bar: 50 μm. Data are presented as means ± SD; *P < 0.05, **P < 0.01, and ***P < 0.001.

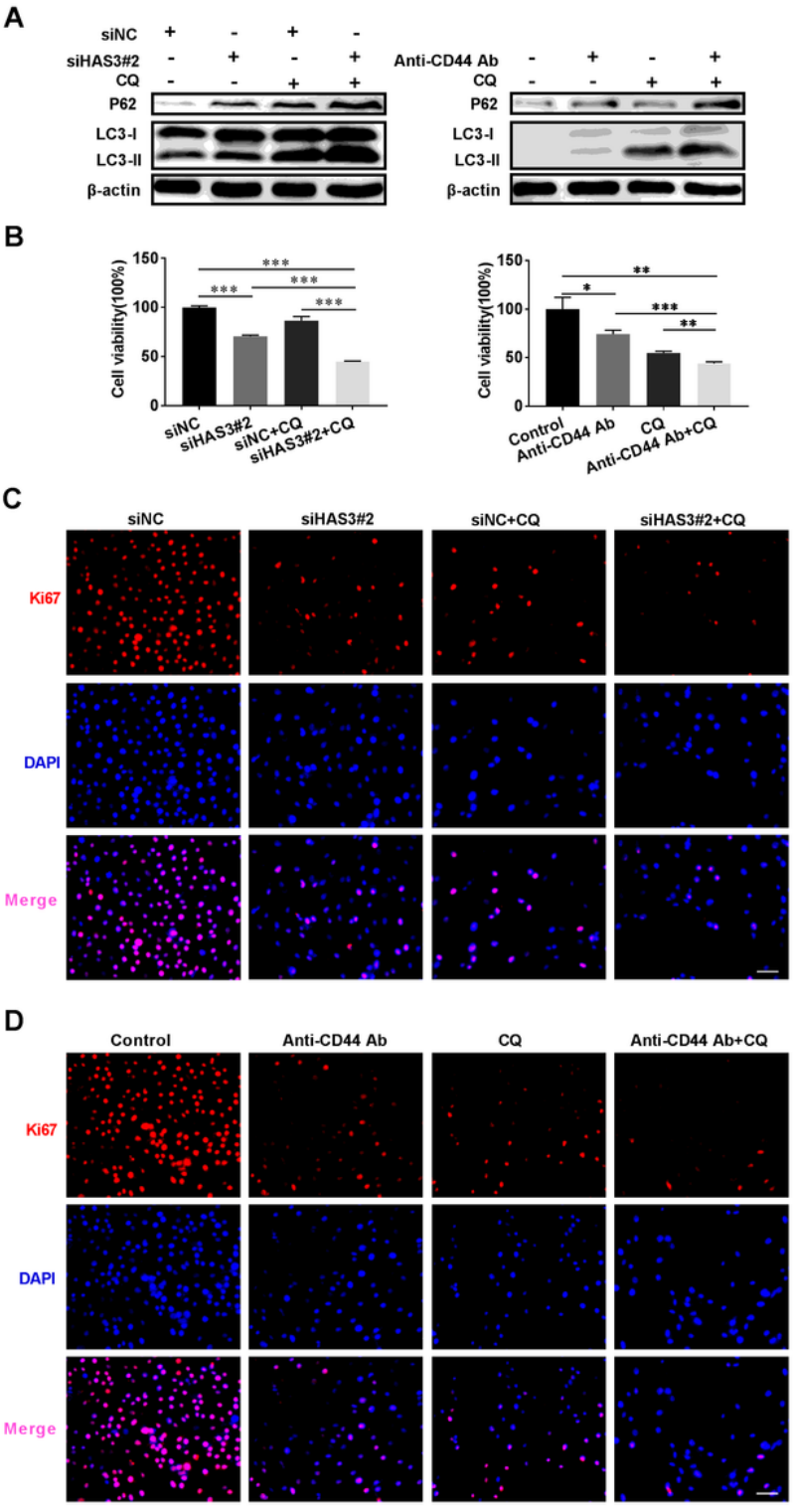

Figure 4

Treatments interfering with HAS3 and CD44 combined with autophagy inhibitors exert synergistic effects on glioma cell viability and autophagy levels. (A) Relative levels of the P62 and LC3 proteins in U251 glioma cells transfected with the HAS3 siRNA or cultured with the CD44 antibody, followed by treatment with CQ (30 mmol/L) for 48 h. (B) Viability of U251 glioma cells transfected with the HAS3 siRNA or cultured with the CD44 antibody, followed by treatment with CQ (30 mmol/L) for 48 h. (C-D) Levels of the

Ki67 protein in U251 glioma cells were detected using immunofluorescence staining after transfection with the HAS3 siRNA or culture with CD44 antibody, followed by treatment with CQ (30 mmol/L) for 48 h. Scale bar: 50 μm. Data are presented as means ± SD; *P < 0.05, **P < 0.01, and ***P < 0.001.

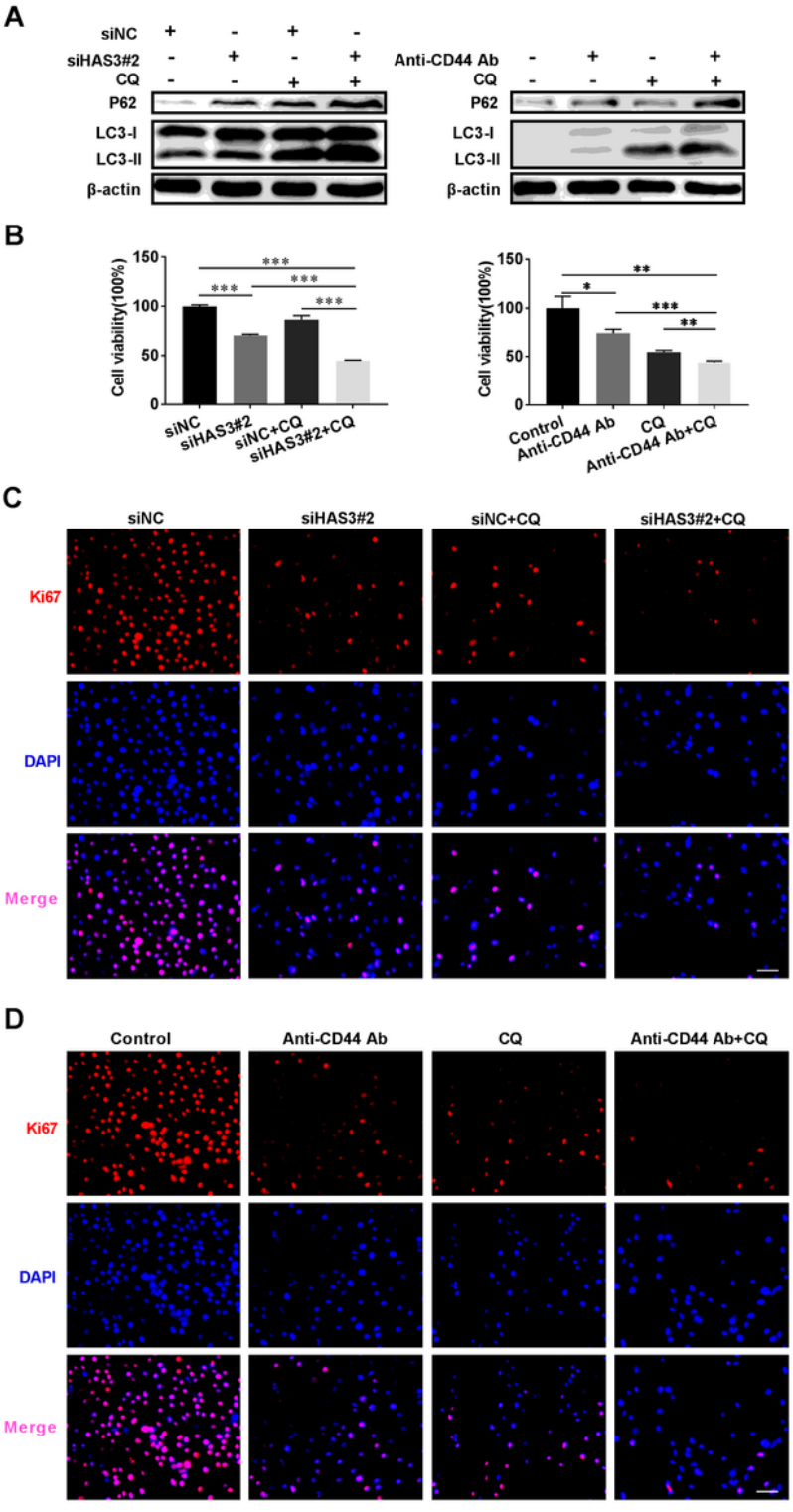

Figure 4

Treatments interfering with HAS3 and CD44 combined with autophagy inhibitors exert synergistic effects on glioma cell viability and autophagy levels. (A) Relative levels of the P62 and LC3 proteins in U251

glioma cells transfected with the HAS3 siRNA or cultured with the CD44 antibody, followed by treatment with CQ (30 mmol/L) for 48 h. (B) Viability of U251 glioma cells transfected with the HAS3 siRNA or cultured with the CD44 antibody, followed by treatment with CQ (30 mmol/L) for 48 h. (C-D) Levels of the Ki67 protein in U251 glioma cells were detected using immunofluorescence staining after transfection with the HAS3 siRNA or culture with CD44 antibody, followed by treatment with CQ (30 mmol/L) for 48 h. Scale bar: 50 μm. Data are presented as means ± SD; *P < 0.05, **P < 0.01, and ***P < 0.001.

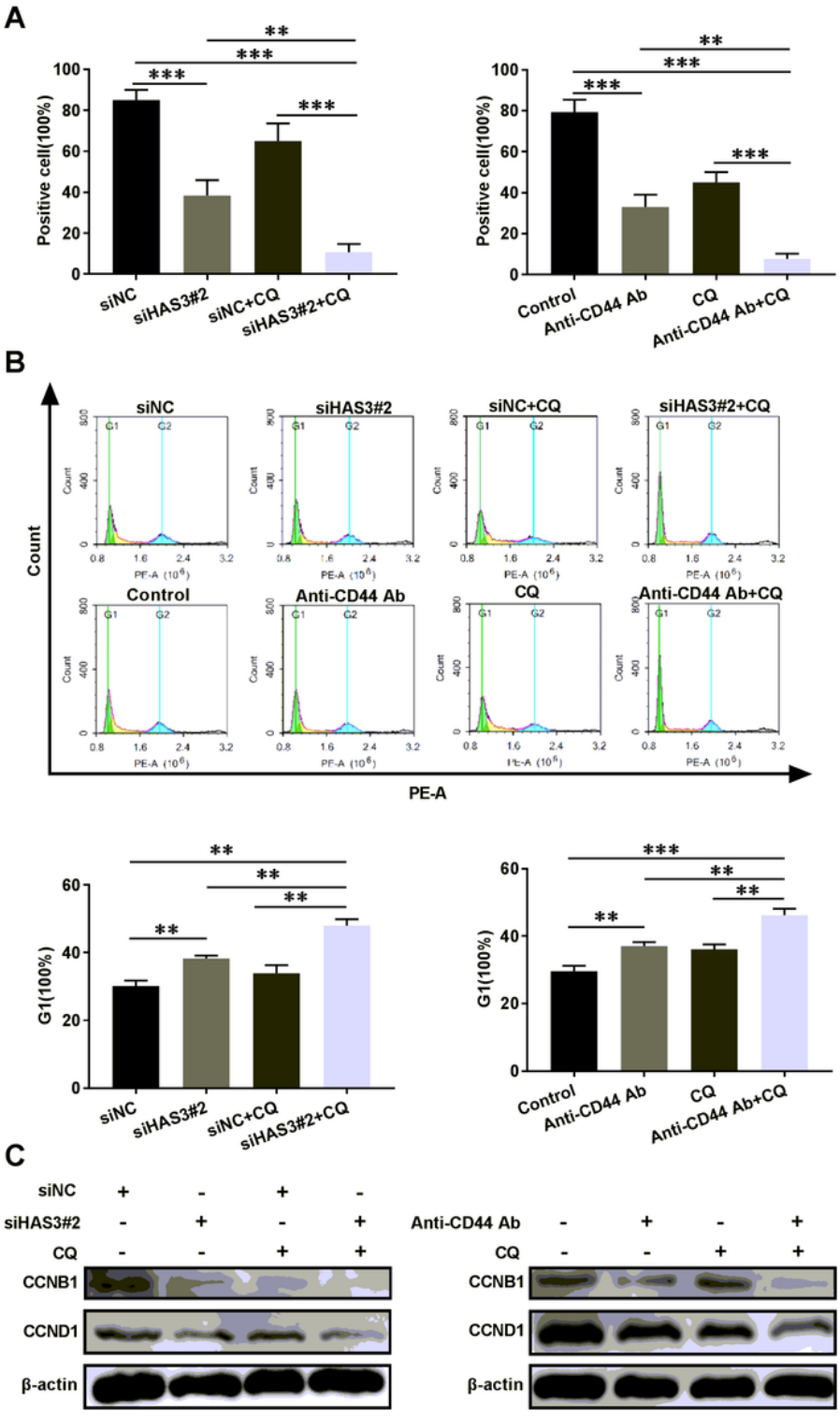

Figure 5

Treatments interfering with HAS3 and CD44 combined with autophagy inhibitors has a synergistic effect on the glioma cell cycle. (A) The percentage of Ki67-positive U251 glioma cells was detected using immunofluorescence staining after transfection with the HAS3 siRNA or culture with the CD44 antibody, followed by treatment with CQ (30 mmol/L) for 48 h. (B) The cell cycle of U251 glioma cells was detected using flow cytometry after transfection with the HAS3 siRNA or culture with the CD44 antibody, followed by treatment with CQ (30 mmol/L) for 48 h. (green: G0-G1, yellow: S, and blue: G2-M). (C) Relative levels of the CCNB1 and CCND1 proteins in U251 glioma cells transfected with the HAS3 siRNA or cultured with the CD44 antibody, followed by treatment with CQ (30 mmol/L) for 48 h. Data are presented as means ± SD; *P < 0.05, **P < 0.01, and ***P < 0.001.

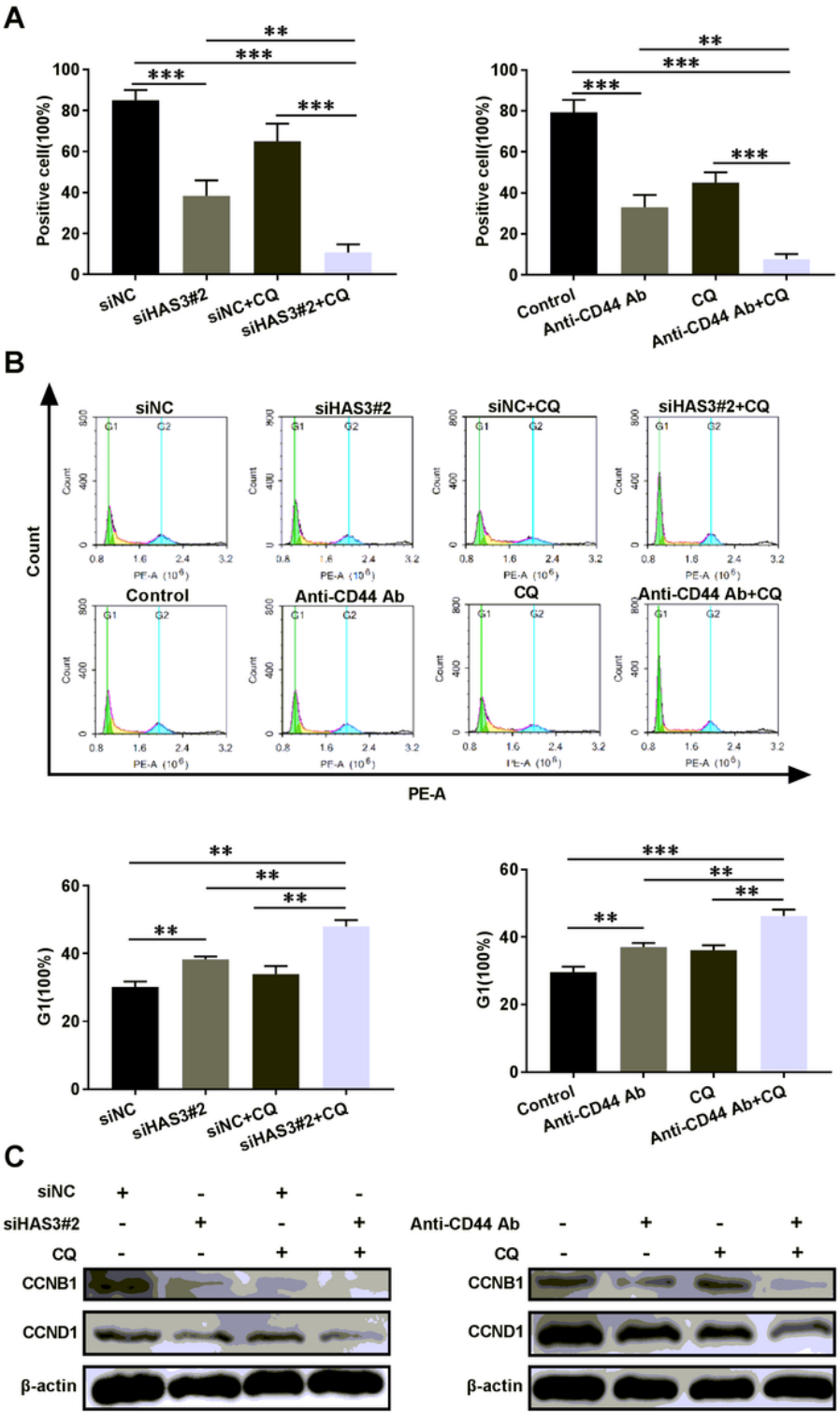

Figure 5

Treatments interfering with HAS3 and CD44 combined with autophagy inhibitors has a synergistic effect on the glioma cell cycle. (A) The percentage of Ki67-positive U251 glioma cells was detected using immunofluorescence staining after transfection with the HAS3 siRNA or culture with the CD44 antibody, followed by treatment with CQ (30 mmol/L) for 48 h. (B) The cell cycle of U251 glioma cells was detected using flow cytometry after transfection with the HAS3 siRNA or culture with the CD44 antibody, followed

by treatment with CQ (30 mmol/L) for 48 h. (green: G0-G1, yellow: S, and blue: G2-M). (C) Relative levels of the CCNB1 and CCND1 proteins in U251 glioma cells transfected with the HAS3 siRNA or cultured with the CD44 antibody, followed by treatment with CQ (30 mmol/L) for 48 h. Data are presented as means ± SD; *P < 0.05, **P < 0.01, and ***P < 0.001.

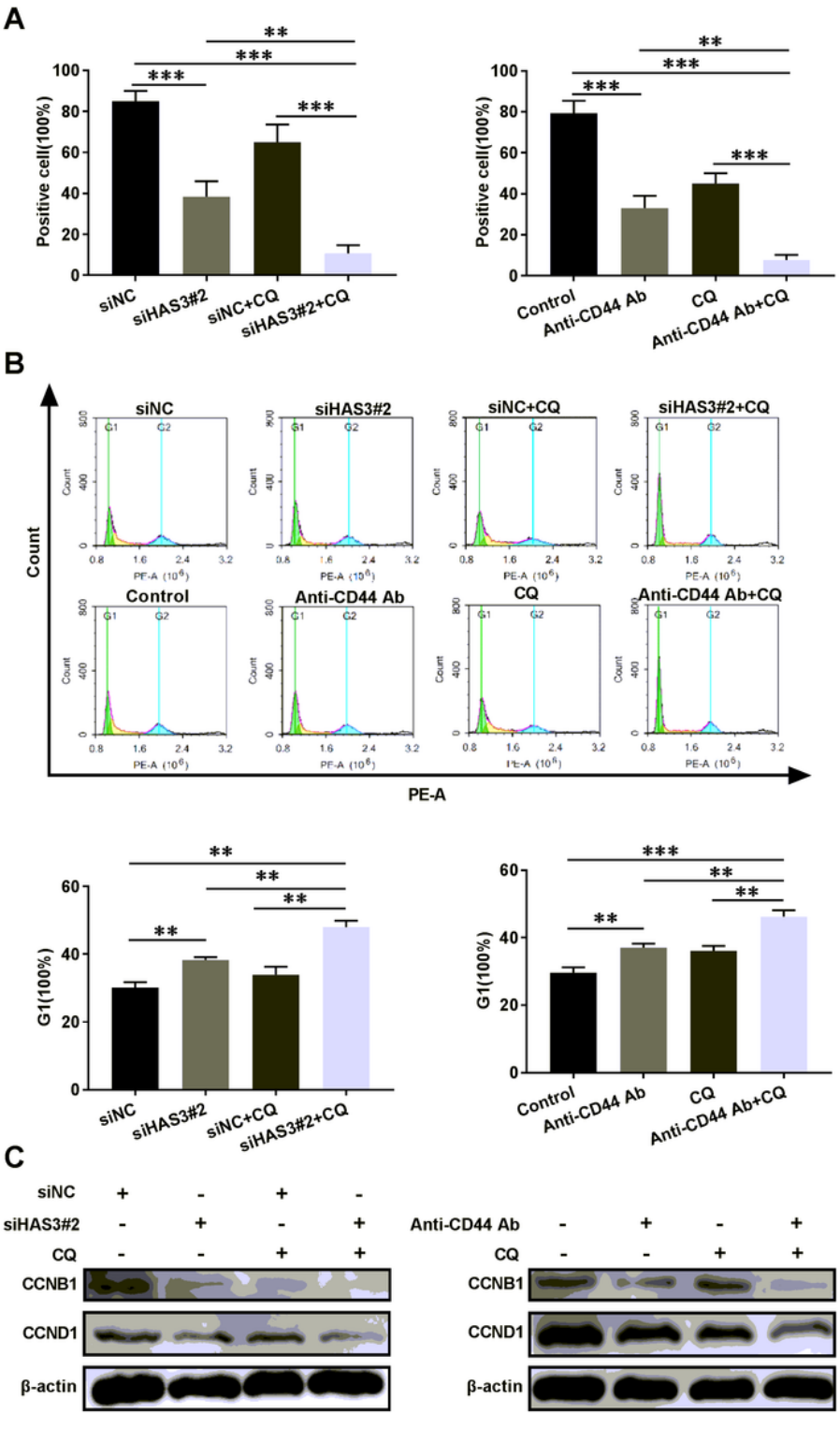

Figure 5

Treatments interfering with HAS3 and CD44 combined with autophagy inhibitors has a synergistic effect on the glioma cell cycle. (A) The percentage of Ki67-positive U251 glioma cells was detected using immunofluorescence staining after transfection with the HAS3 siRNA or culture with the CD44 antibody, followed by treatment with CQ (30 mmol/L) for 48 h. (B) The cell cycle of U251 glioma cells was detected using flow cytometry after transfection with the HAS3 siRNA or culture with the CD44 antibody, followed by treatment with CQ (30 mmol/L) for 48 h. (green: G0-G1, yellow: S, and blue: G2-M). (C) Relative levels of the CCNB1 and CCND1 proteins in U251 glioma cells transfected with the HAS3 siRNA or cultured with the CD44 antibody, followed by treatment with CQ (30 mmol/L) for 48 h. Data are presented as means ± SD; *P < 0.05, **P < 0.01, and ***P < 0.001.

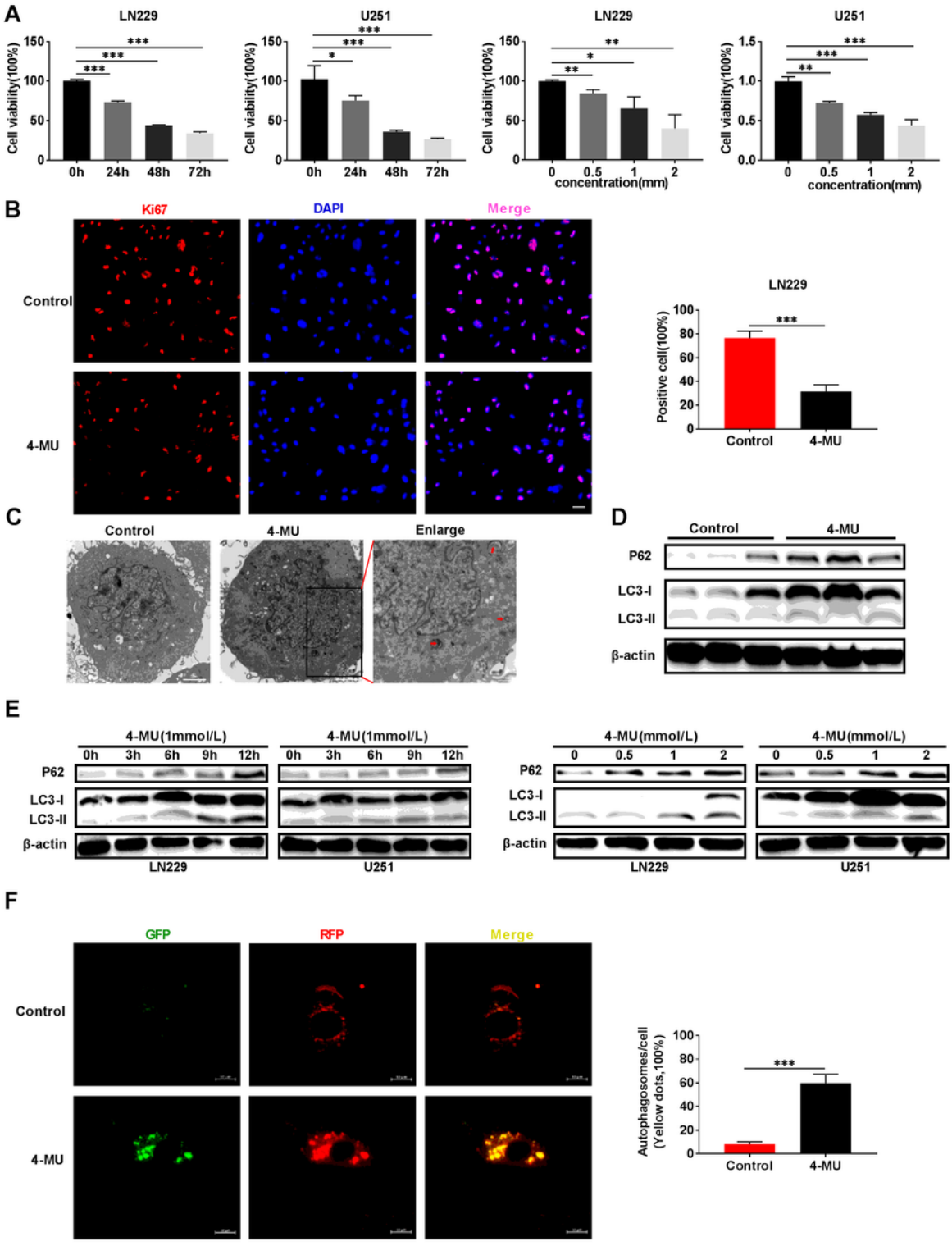

Figure 6

4-MU decreases glioma viability and block autophagy flux. (A) Viability of U251 and LN229 glioma cells treated with 4-MU (1 mmol/L) for 0, 24, 48, and 72 h. Viability of U251 and LN229 glioma cells treated with different concentrations of 4-MU (0, 0.5, 1, or 2 mmol/L) for 48 h. (B) Levels of the Ki67 protein in LN229 glioma cells were detected using immunofluorescence staining after treatment with 4-MU for 48 h. Scale bar: 50 μm. (C) TEM images of U251 glioma cells treated with 4-MU for 48 h. The scale bars

represent 2 μm in the original image and 0.8 μm in the enlarged image. (D) Relative levels of the P62 and LC3 proteins in the orthotopic xenograft tumors from the control and 4-MU treatment groups. (E) Relative levels of the P62 and LC3 proteins in U251 and LN229 glioma cell lines treated with 4-MU (1 mmol/L) for 0, 3, 6, 9, and 12 h. Relative levels of the P62 and LC3 proteins in U251 and LN229 glioma cell lines treated with different concentrations of 4-MU (0, 0.5, 1, or 2 mmol/L) for 48 h. (F) GFP-RFP-LC3 fluorescence assays of U251 glioma cells treated with 4-MU for 48 h. Scale bar: 10 μm. Data are presented as means ± SD; *P < 0.05, **P < 0.01, and ***P < 0.001.

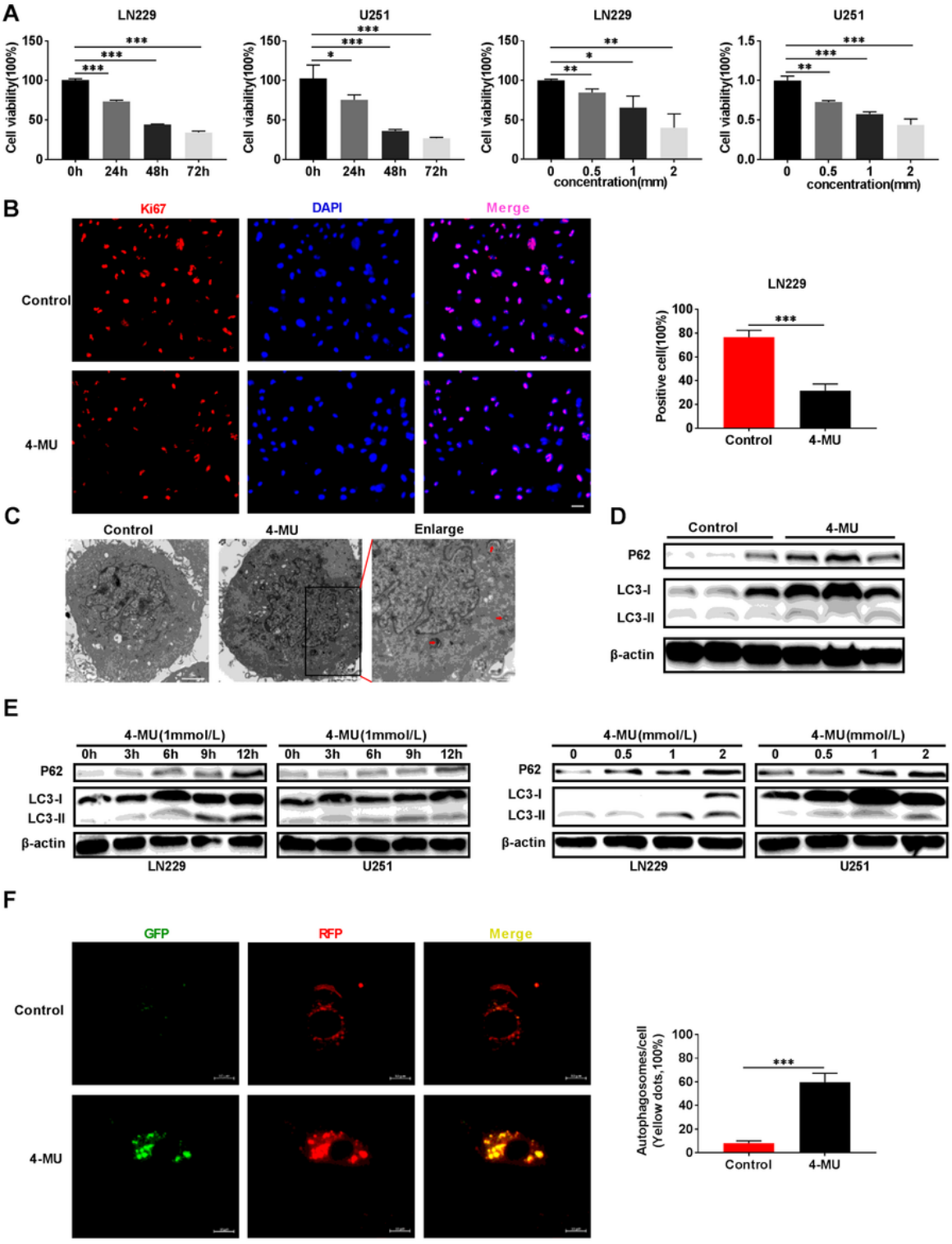

Figure 6

4-MU decreases glioma viability and block autophagy flux. (A) Viability of U251 and LN229 glioma cells treated with 4-MU (1 mmol/L) for 0, 24, 48, and 72 h. Viability of U251 and LN229 glioma cells treated with different concentrations of 4-MU (0, 0.5, 1, or 2 mmol/L) for 48 h. (B) Levels of the Ki67 protein in LN229 glioma cells were detected using immunofluorescence staining after treatment with 4-MU for 48 h. Scale bar: 50 μm. (C) TEM images of U251 glioma cells treated with 4-MU for 48 h. The scale bars represent 2 μm in the original image and 0.8 μm in the enlarged image. (D) Relative levels of the P62 and LC3 proteins in the orthotopic xenograft tumors from the control and 4-MU treatment groups. (E) Relative levels of the P62 and LC3 proteins in U251 and LN229 glioma cell lines treated with 4-MU (1 mmol/L) for 0, 3, 6, 9, and 12 h. Relative levels of the P62 and LC3 proteins in U251 and LN229 glioma cell lines treated with different concentrations of 4-MU (0, 0.5, 1, or 2 mmol/L) for 48 h. (F) GFP-RFP-LC3 fluorescence assays of U251 glioma cells treated with 4-MU for 48 h. Scale bar: 10 μm. Data are presented as means ± SD; *P < 0.05, **P < 0.01, and ***P < 0.001.

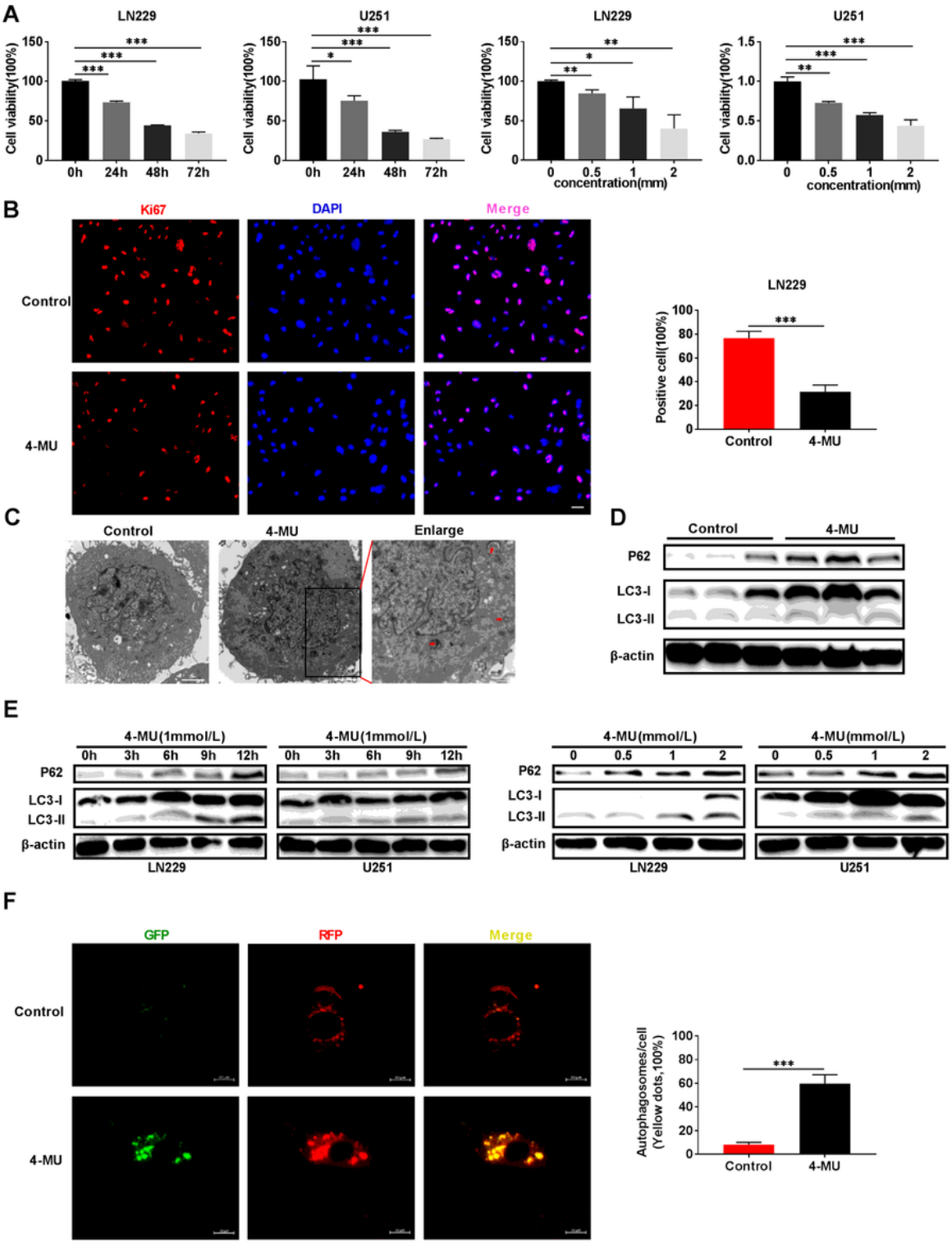

Figure 6

4-MU decreases glioma viability and block autophagy flux. (A) Viability of U251 and LN229 glioma cells treated with 4-MU (1 mmol/L) for 0, 24, 48, and 72 h. Viability of U251 and LN229 glioma cells treated with different concentrations of 4-MU (0, 0.5, 1, or 2 mmol/L) for 48 h. (B) Levels of the Ki67 protein in LN229 glioma cells were detected using immunofluorescence staining after treatment with 4-MU for 48 h. Scale bar: 50 μm. (C) TEM images of U251 glioma cells treated with 4-MU for 48 h. The scale bars

represent 2 μm in the original image and 0.8 μm in the enlarged image. (D) Relative levels of the P62 and LC3 proteins in the orthotopic xenograft tumors from the control and 4-MU treatment groups. (E) Relative levels of the P62 and LC3 proteins in U251 and LN229 glioma cell lines treated with 4-MU (1 mmol/L) for 0, 3, 6, 9, and 12 h. Relative levels of the P62 and LC3 proteins in U251 and LN229 glioma cell lines treated with different concentrations of 4-MU (0, 0.5, 1, or 2 mmol/L) for 48 h. (F) GFP-RFP-LC3 fluorescence assays of U251 glioma cells treated with 4-MU for 48 h. Scale bar: 10 μm. Data are presented as means ± SD; *P < 0.05, **P < 0.01, and ***P < 0.001.

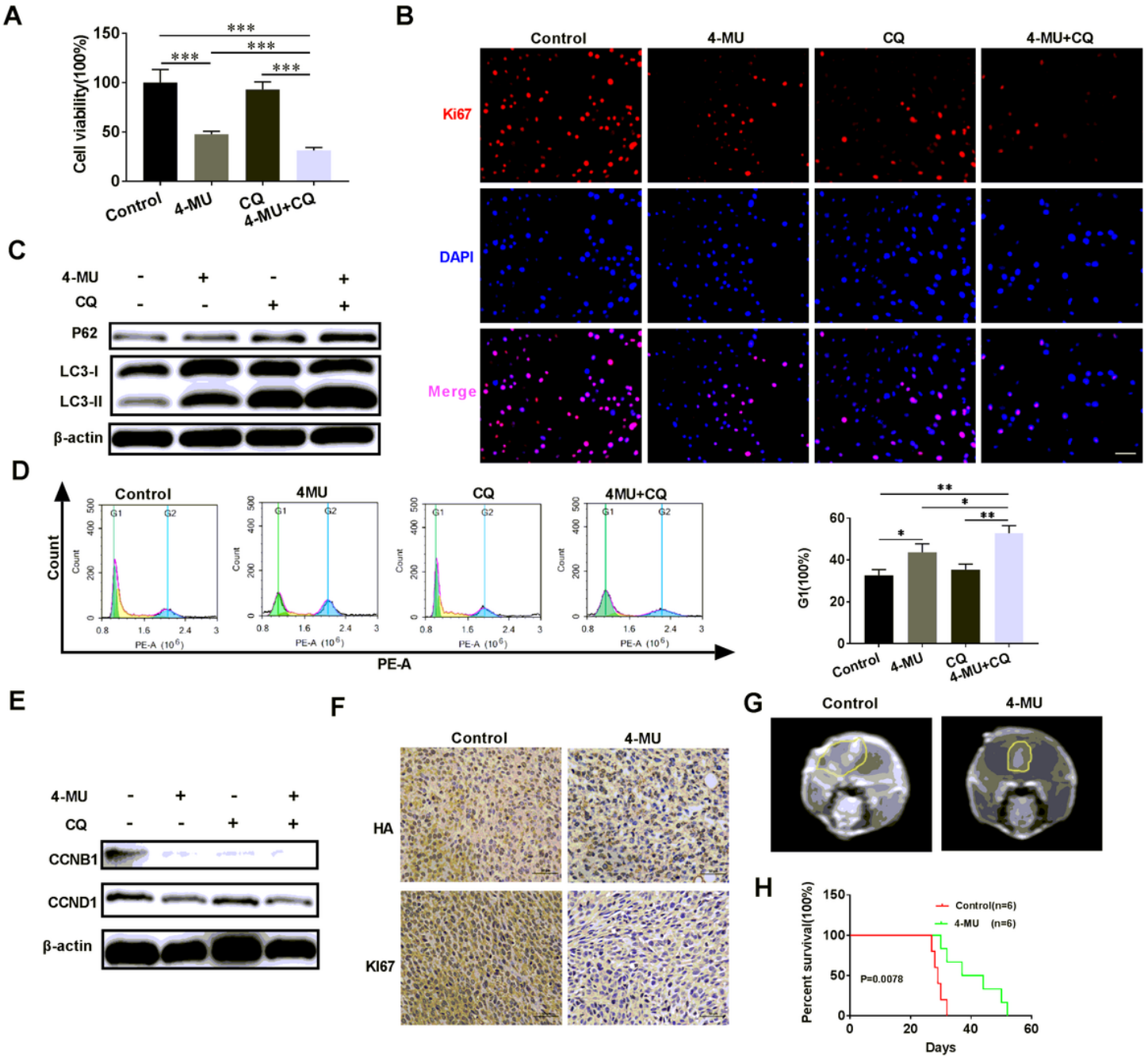

Figure 7

4-MU inhibits glioma growth in vivo and, when combined with autophagy inhibitors, exerts synergistic effects on glioma cell viability, autophagy levels and the cell cycle. (A)Viability of U251 glioma cells cultured with 4-MU, followed by treatment with CQ (30 mmol/L) for 48 h. (B)Levels of the Ki67 protein in U251 glioma cells were detected using immunofluorescence staining after culture with 4-MU, followed by treatment with CQ (30 mmol/L) for 48 h. (C)Relative levels of the P62 and LC3 proteins in U251 glioma cells cultured with 4-MU, followed by treatment with CQ (30 mmol/L) for 48 h. Scale bar: 50 μm. (D) The cell cycle was detected in U251 glioma cells using flow cytometry after culture with 4-MU, followed by treatment with CQ (30 mmol/L) for 48 h (green: G0-G1, yellow: S, and blue: G2-M). (E) Relative levels of the CCNB1 and CCND1 proteins in U251 glioma cells cultured with 4-MU, followed by treatment with CQ (30 mmol/L) for 48 h. (F) Representative images of IHC staining for Ki67 and HA in the orthotopic xenograft tumors from the control and 4-MU treatment groups. Scale bar: 50 μm. (G-H) Representative MRIs of orthotopic xenograft tumors and survival curves of the control and 4-MU treatment groups. P: P-value for the comparison of the control and 4-MU groups. Data are presented as means ± SD; *P < 0.05, **P < 0.01, and ***P < 0.001.

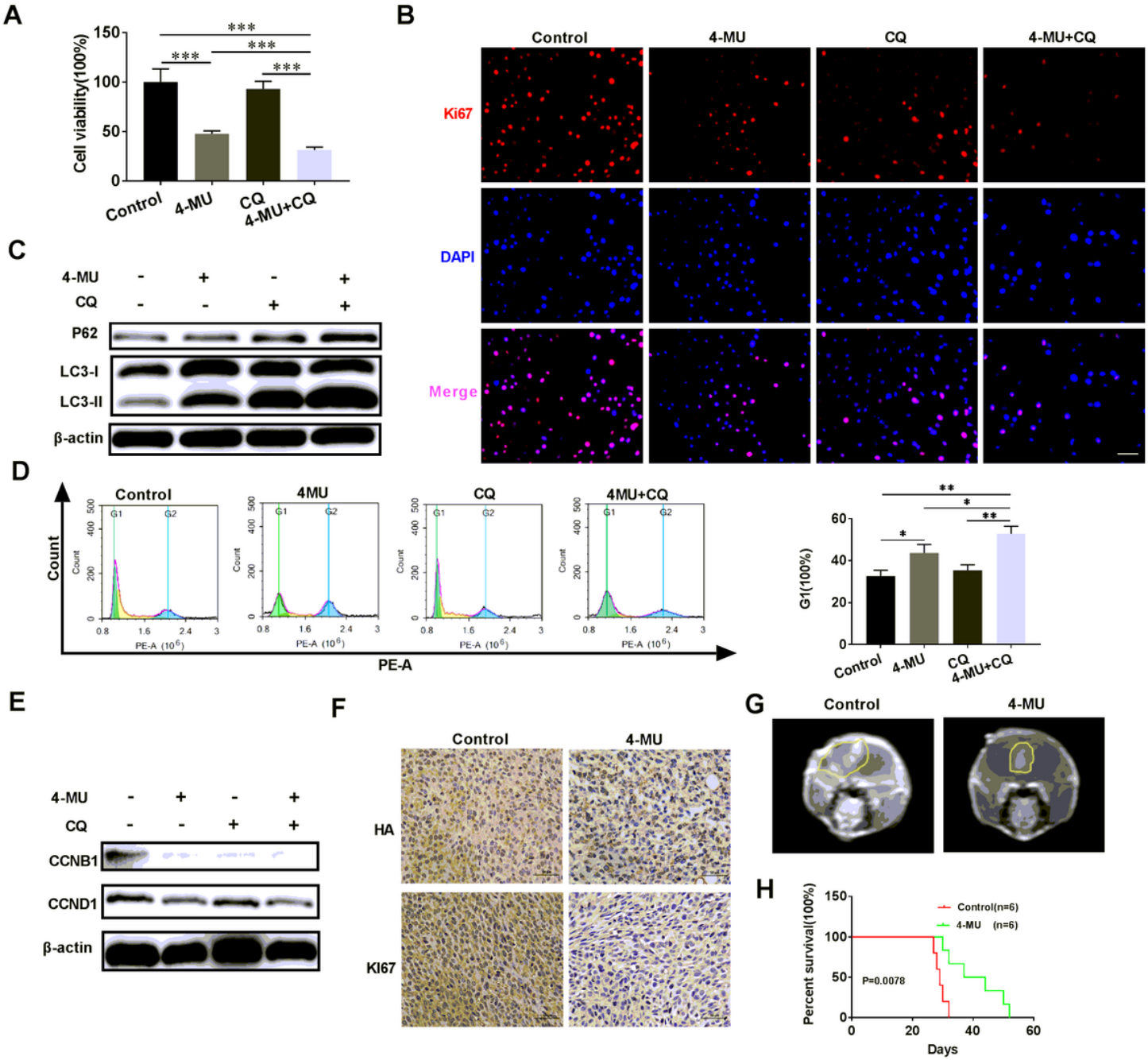

Figure 7

4-MU inhibits glioma growth in vivo and, when combined with autophagy inhibitors, exerts synergistic effects on glioma cell viability, autophagy levels and the cell cycle. (A)Viability of U251 glioma cells cultured with 4-MU, followed by treatment with CQ (30 mmol/L) for 48 h. (B)Levels of the Ki67 protein in U251 glioma cells were detected using immunofluorescence staining after culture with 4-MU, followed by treatment with CQ (30 mmol/L) for 48 h. (C)Relative levels of the P62 and LC3 proteins in U251 glioma cells cultured with 4-MU, followed by treatment with CQ (30 mmol/L) for 48 h. Scale bar: 50 μm. (D) The cell cycle was detected in U251 glioma cells using flow cytometry after culture with 4-MU, followed by treatment with CQ (30 mmol/L) for 48 h (green: G0-G1, yellow: S, and blue: G2-M). (E) Relative levels of

the CCNB1 and CCND1 proteins in U251 glioma cells cultured with 4-MU, followed by treatment with CQ (30 mmol/L) for 48 h. (F) Representative images of IHC staining for Ki67 and HA in the orthotopic xenograft tumors from the control and 4-MU treatment groups. Scale bar: 50 μm. (G-H) Representative MRIs of orthotopic xenograft tumors and survival curves of the control and 4-MU treatment groups. P: P-value for the comparison of the control and 4-MU groups. Data are presented as means ± SD; *P < 0.05, **P < 0.01, and ***P < 0.001.

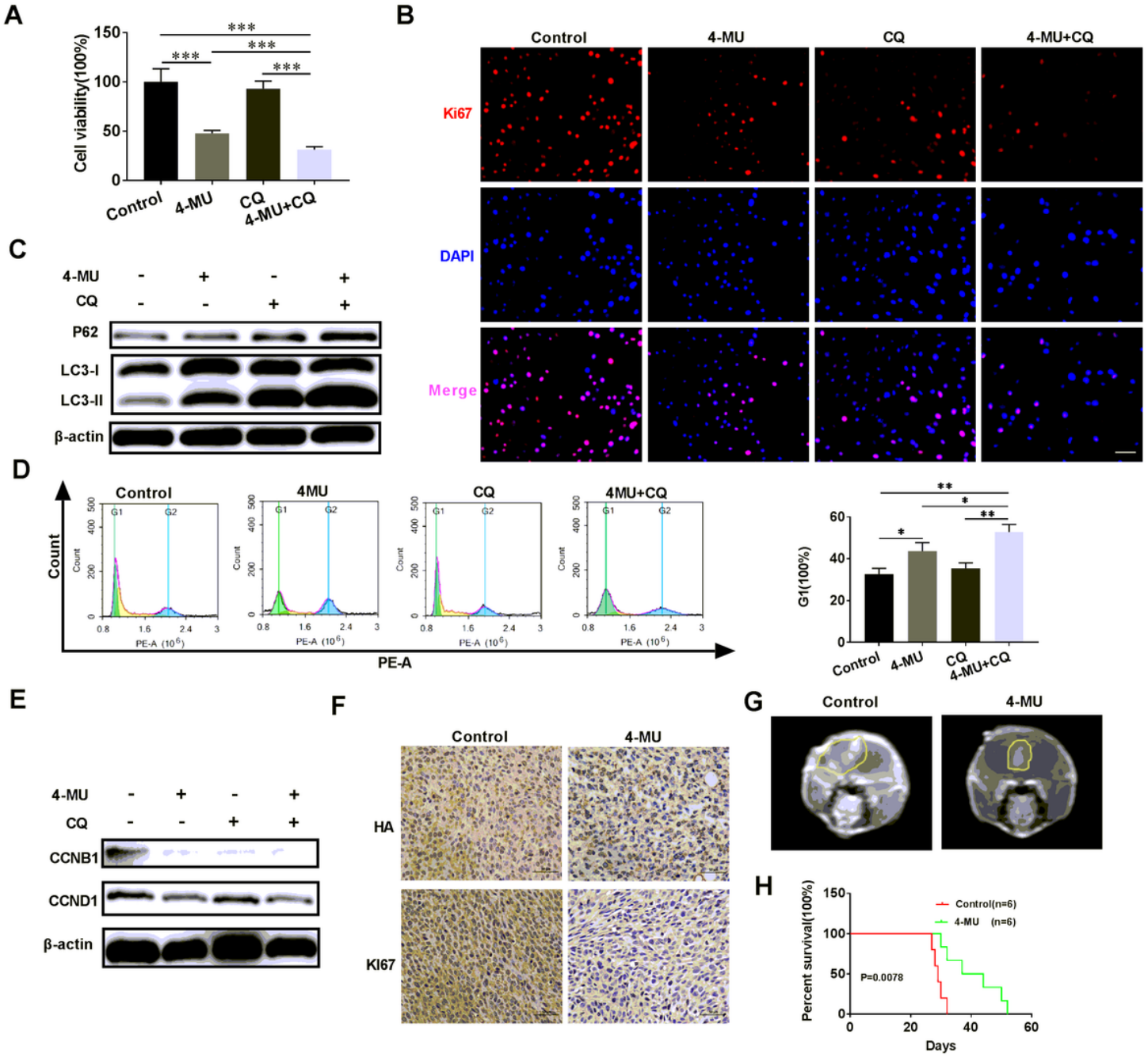

Figure 7

4-MU inhibits glioma growth in vivo and, when combined with autophagy inhibitors, exerts synergistic effects on glioma cell viability, autophagy levels and the cell cycle. (A)Viability of U251 glioma cells

cultured with 4-MU, followed by treatment with CQ (30 mmol/L) for 48 h. (B)Levels of the Ki67 protein in U251 glioma cells were detected using immunofluorescence staining after culture with 4-MU, followed by treatment with CQ (30 mmol/L) for 48 h. (C)Relative levels of the P62 and LC3 proteins in U251 glioma cells cultured with 4-MU, followed by treatment with CQ (30 mmol/L) for 48 h. Scale bar: 50 μm. (D) The cell cycle was detected in U251 glioma cells using flow cytometry after culture with 4-MU, followed by treatment with CQ (30 mmol/L) for 48 h (green: G0-G1, yellow: S, and blue: G2-M). (E) Relative levels of the CCNB1 and CCND1 proteins in U251 glioma cells cultured with 4-MU, followed by treatment with CQ (30 mmol/L) for 48 h. (F) Representative images of IHC staining for Ki67 and HA in the orthotopic xenograft tumors from the control and 4-MU treatment groups. Scale bar: 50 μm. (G-H) Representative MRIs of orthotopic xenograft tumors and survival curves of the control and 4-MU treatment groups. P: P-value for the comparison of the control and 4-MU groups. Data are presented as means ± SD; *P < 0.05, **P < 0.01, and ***P < 0.001.

Supplementary Files

This is a list of supplementary files associated with this preprint. Click to download.

- Table.docx
- Table.docx
- Table.docx
- SupplementaryFigure3.tif
- SupplementaryFigure3.tif
- SupplementaryFigure3.tif
- SupplementaryFigure2.tif
- SupplementaryFigure2.tif
- SupplementaryFigure2.tif
- SupplementaryFigure1.tif
- SupplementaryFigure1.tif
- SupplementaryFigure1.tif
- supplementfigurelegend.docx
- supplementfigurelegend.docx
- supplementfigurelegend.docx